R. & M. No. 2866
(13, 910, 11,008)
(A.R.C. Technical Report)

MINISTRY OF SUPPLY

AERONAUTICAL RESEARCH COUNCIL
REPORTS AND MEMORANDA

Flutter and Resonance Characteristics of a Model Cantilever Wing Carrying Localised Masses

By

N. C. LAMBOURNE
of the Aerodynamics Division, N.P.L.

NATIONAL AERONAUTICAL ESTABLISHMENT,
25 JUL 1955
LIBRARY

Crown Copyright Reserved

LONDON: HER MAJESTY'S STATIONERY OFFICE
1955
SEVEN SHILLINGS NET

Flutter and Resonance Characteristics of a Model Cantilever Wing Carrying Localised Masses

By

N. C. LAMBOURNE,

of the Aerodynamics Division, N.P.L.

Reports and Memoranda No. 2866*

April, 1951

Summary.—Resonance tests on a model cantilever wing carrying concentrated masses were made in conjunction with the flutter tests of R. & M. 2533[7]. Measurements were made with masses up to approximately five times the mass of the bare wing added at the following positions in the section 0·3 span from the root of the wing:

(i) Externally 0·28*c* ahead of leading edge

(ii) Internally 0·3*c* behind leading edge.

The flutter and resonance characteristics are placed in juxtaposition, and an attempt is made to correlate the two sets of phenomena by means of the Küssner criterion.

The distortion modes of flutter are analysed into normal mode components, and the results suggest that for a wing rigidly fixed at the root and carrying a single concentrated mass the first three normal modes are sufficient to define the flutter mode.

1. *Introduction.*—A knowledge of the natural frequencies and normal modes of an aircraft is important in relation to the estimation of the flutter critical speed, and the value of resonance tests in providing this information has been dealt with elsewhere[1, 2, 3]. Based on experience, qualitative estimations of the flutter properties may be made by an examination of the resonance properties, and at one time in the past, it was common to obtain an approximate value of the critical speed from a simple criterion due to Küssner which required a knowledge of the resonance frequencies and positions of the nodal lines. It is clearly valuable to be able to place, as can be done for experiments with models, the measured flutter characteristics side-by-side with the corresponding resonance data. Jones and Scruton[4] measured the critical speeds of a model wing for various conditions of mass-loading, and in an examination of the effectiveness of Küssner's criterion related these speeds to the still-air resonance frequencies and the positions of the node at the wing tip. A detailed examination of the resonance modes was, however, not made. Hanson and Warlow-Davies[5] and Taylor[6] investigated in detail the effect of concentrated masses representing wing engines on the resonances of a structural model of a wing, but with the type of model used no knowledge of the flutter characteristics could be obtained. Lambourne and Weston[7] investigated experimentally the influence of masses representing both engines and fuel tanks on the flexure-torsion flutter characteristics of a model wing. A detailed account of resonance tests and stiffness measurements made on the same wing is given in an unpublished paper[8], but some of the more important results of these tests are included in the present report.

*A.R.C. 13,910 and parts of A.R.C. 11,008.

Published with the permission of the Director, National Physical Laboratory.

The modes of distortion during flutter were measured for a few cases of mass-loading at an external (representing leading-edge engines), and at an internal location (representing fuel-tank and jet-engine installation), and it was for these positions of the additional mass that the resonance characteristics were measured. In addition, the elastic properties of the wing were measured in the form of flexibility coefficients, which together with a detailed specification of the mass distribution, provide basic data for theoretical calculations, the results of which have been issued in unpublished reports by Frazer[9, 10].

In practice a combination of two or more of the normal modes obtained from resonance tests is frequently used as a basis for flutter calculations, and the question arises as to how many and which normal modes are necessary to give a satisfactory estimate of the critical speed. For the wing of this report some useful information in this connection is obtained by determining the amount of each normal mode required to build up the measured flutter mode of distortion. For this purpose the measured flutter modes are analysed in terms of the normal mode components.

2. *The Model Wing.*—A detailed description of the wing construction appears in Ref. 7, whilst Table 1 of the present report gives the final mass distribution of the wing in the form of the masses, mass moments, and inertias associated with each rib. This table is based on the inventory of the mass and the position of each component part, which was kept during the course of construction. Table 2 gives the masses and inertias of the steel fittings (the engine mountings) which could be attached to certain ribs to support the leading castings representing the external engine masses.

3. *Flexibility Coefficients.*—The elastic properties of the wing were measured immediately after the wing was constructed and before any of the resonance or flutter tests were carried out. Owing to variations in the wing stiffnesses that occurred during the subsequent tests, and which are dealt with in section 4, the measured flexibility coefficients are not strictly applicable to either the resonance or the flutter tests but they do serve as a standard basis for calculations. One would expect that, although general changes in the wing stiffness occurred, the stiffness distribution over the wing would remain approximately the same, so that calculated resonance and flutter characteristics based on the initial stiffness and inertia data should show qualitative if not quantitative agreement with experimental results.

Measurements were made of

(i) Flexural displacements z, the linear normal displacements at the transverse reference axis OY situated at $0{\cdot}3c$ from the leading edge.

(ii) Twists θ at chordwise sections.

due to

(a) loads applied at the reference axis OY.

(b) twisting couples in planes normal to axis OY.

Mean flexibilities for each case of loading were obtained and the final results were put into the form of four matrices of flexibility coefficients as follows :

$\mathscr{A}$ $(\eta\eta')$ the flexure at η due to unit force at η',

$\mathscr{B}$ $(\eta\eta')$ the flexure at η due to unit couple at η',

$\mathscr{C}$ $(\eta\eta')$ the twist at η due to unit couple at η',

$\mathscr{D}$ $(\eta\eta')$ the twist at η due to unit force at η',

where $\eta = y/s$ the spanwise co-ordinate.

By the Elasticity Reciprocal Theorem, matrices $\mathscr{A}$ and $\mathscr{C}$ should each be symmetrical, and $\mathscr{D}$ should be the transpose of $\mathscr{B}$.

Thus :

$$\mathscr{A}(\eta\eta') = \mathscr{A}(\eta'\eta)\ ;\quad \mathscr{B}(\eta\eta') = \mathscr{D}(\eta'\eta)\ ;\quad \mathscr{C}(\eta\eta') = \mathscr{C}(\eta'\eta).$$

The experimental results were found to accord well with the theory.

The matrices given in Tables 3, 4 and 5 provide a standard set of flexibility coefficients for use in the calculation of critical speeds, etc., and represent smoothed mean values. The matrix $\mathscr{A}$ was obtained as the mean of the experimental matrix $\mathscr{A}$ and its transpose, while matrix $\mathscr{C}$ was obtained on a similar basis. The matrix $\mathscr{B}$ is the mean of the experimental matrix $\mathscr{B}$ and the transpose of the experimental matrix $\mathscr{D}$.

The position of the flexural centre at any section η is given by

$$x = -\mathscr{B}(\eta\eta)/\mathscr{C}(\eta\eta) = -\mathscr{D}(\eta\eta)/\mathscr{C}(\eta\eta)$$

where x is the distance aft of the reference axis. Values of x obtained from the standard set of flexibility coefficients have been used to obtain Table 6 which gives the distances of the flexural centres behing the leading edge in terms of the local chord.

4. *Change of Wing Stiffnesses during the Tests.*—Some difficulty was experienced due to the pronounced temperature variation of the building in which the stiffness tests were made, a change of 14 deg C being not uncommon during a hot day. It was found that the torsional stiffness of the wing as measured at the tip section decreased with increasing temperature at a rate of approximately 0·5 per cent per deg C, but no appreciable variation of the flexural stiffness was observed. Independent evidence was obtained of temperature change affecting the torsional properties of wood by a simple experiment on a spruce rod, and the results were in agreement with those of some early experiments of Griffiths and Wigley[11].

To obtain consistent results in the measurement of flexibility coefficients, as far as possible all the records were taken while the ambient temperature was approximately 16 deg C.

It was also found that the stiffness of the wing decreased during a preliminary set of resonance tests carried out prior to the flutter tests and a further decrease was noticed during the flutter tests (*see* Ref. 7). Remeasurement of the stiffnesses just before the main series of resonance tests indicated that they had increased whilst the wing had been stored. Table 7 gives the wing stiffnesses together with the flutter critical speeds and frequencies of the bare wing as measured from time to time.

5. *Resonance Tests.*—A detailed account of the resonance tests and the results are contained in Ref. 8, and only a brief account of these experiments is given in the present report.

The wing was excited through a spring by a reciprocating member driven by an electric motor, the resonance amplitudes at selected stations along the leading and trailing edges being recorded photographically. Due to the special form of construction (*see* Ref. 7) it is possible to make the assumption that chordwise sections of the wing do not change their shape, so that the motion of a section may be defined in terms of flexure and torsion components.

$$\phi = \Phi \sin pt$$

$$\theta = \Theta \sin (pt + \varepsilon) \quad \ldots \quad \text{(see Fig. 1.)}$$

At resonance ε is approximately 0 or π. The position of the node in the section is given by

$$X = -(\Phi/\Theta)s \quad \ldots \quad \text{(see Fig. 1.)}$$

Values of Φ, Θ and X for a number of spanwise stations were deduced from the recorded deflections of the leading and trailing edges. It will be noted that the nodes are virtual centres of rotation of the sections, and for this reason the ' nodal lines ' shown in the diagrams have in some cases been extended to positions that do not lie within the wing area.

The nodal lines are plotted on diagrams having a linear scale in the spanwise direction (η) and a scale $x' = n \tanh (x/n)$ in the chordwise direction, so that it is possible to include nodal lines far removed from the wing, the value of n being chosen to leave the plan form of the wing almost unchanged.

Resonance frequences and modes were measured for various values of mass loading at the following positions :

(i) Externally $\eta = 0{\cdot}3$, $0{\cdot}28c$ ahead of leading edge ($x = -0{\cdot}58c$),

(ii) Internally $\eta = 0{\cdot}3$, $0{\cdot}30c$ behind the leading edge ($x = 0$).

These were the loading positions most extensively used in the flutter tests, and those for which the flutter modes were measured.

The method of mass-loading is explained in Ref. 7, and, as in the flutter tests, the mass range was $\mu = 0$ to 2 slugs, with an additional condition representing $\mu = \infty$.

The Case of $\mu = \infty$. For any position of mass-loading the first natural frequency tends to zero as the added mass μ tends to ∞, so that ultimately all the inertia forces on the wing would vanish except that due to μ itself. Thus the first normal mode for $\mu = \infty$ would be identical with the distortion mode for static loading at the point of application of μ ; it may therefore be obtained by a simple calculation from the measured flexibility coefficients. However, as a check on these coefficients, the static modes were measured for direct loading at the mass-loading positions, and the results were found to compare favourably with those derived from the flexibility coefficients.

As the other natural frequencies do not become evanescent as μ tends to ∞, the mass-loading position becomes a node for those oscillations, and the hypothetical condition $\mu = \infty$ can be represented by preventing the motion of the point of mass loading. In the tests this was carried out by using vertical straining wires connected to the wing as described in Ref. 7.

A few remarks on the results of the tests now follow :

Mass-loading Externally.—The variation of the resonance frequencies with added mass are shown in Fig. 10b, whilst the positions of the nodal lines are shown in Figs. 2 to 5. The first resonance frequency decreases with increasing mass over the whole of the experimental range, whilst the second, third and fourth resonance frequency curves become asymptotic at successively smaller values of μ.

Mass-loading Internally.—The resonance frequencies are shown in Fig. 11b, and the positions of the nodal lines are shown in Figs. 6 to 9. No nodal-line diagram is included for the first resonance, since for all cases of mass-loading the motion was approximately pure flexure, and the ' nodal lines ' were far distant from the wing.

The first resonance frequency decreases only slightly as μ is increased over the experimental range. The second resonance frequency remains approximately constant up to $\mu \simeq 0{\cdot}5$ slug and then decreases, whilst the third resonance frequency, on the other hand, decreases with increase of μ for small values, and remains almost constant for $\mu > 1{\cdot}0$ slug. The second and third resonance frequency curves approach one another in the region of $\mu \simeq 0{\cdot}5$ slug and they have the appearance of almost intersecting. In fact from the experiments themselves it is not perfectly clear that these two curves do not intersect, for in the region where the two frequencies are close together, large phase differences were present and it was very difficult to define the precise resonance conditions. However, theoretical calculations made by Frazer[9] for an equivalent ideal wing do not give a point of intersection, and the experimental points have been drawn accordingly. It will be noticed that the asymptotic value of the third resonance frequency as μ tends to ∞ is approximately the same as the value of the second resonance frequency when $\mu = 0$.

The second resonance is predominantly torsional in character until $\mu \simeq 0{\cdot}6$ slug but for larger additional masses it tends to a flexural overtone type. On the other hand, for $\mu < 0{\cdot}5$ slug the third resonance has the character of a flexural overtone whilst for $\mu > 1{\cdot}0$ slug the oscillation

is predominantly torsional and has the character, as well as the frequency, appropriate to the second resonance for $\mu = 0$. Viewed in a somewhat different manner, and in conjunction with the changes in the second resonance, the character of the fundamental torsion resonance may be regarded as persisting whilst mass is added at the reference axis. This is only to be expected since the position of the nodal line for this type of oscillation passes approximately through the mass loading position. Initially for $\mu = 0$ the fundamental torsional type of oscillation is associated with the second frequency, but with increase of μ the frequency of the flexural overtone oscillation falls below the frequency of fundamental torsion, and the latter type of oscillation becomes promoted to the third frequency.

It has already been mentioned that it was difficult to obtain clearly defined resonances in the region where the second and third resonance frequency curves approach one another closely, and the results which were obtained give little information of the manner in which the change in the characteristics of the third resonance occurs. A sequence of nodal line patterns to show a possible way in which this change-over takes place is suggested in Fig. 8.

6. *Comparison of Resonance and Flutter Results.*—To correlate the resonance and flutter phenomena the variations with added mass of the following quantities are shown in a single diagram :

Resonance

Position of nodal line for 2nd and 3rd resonances

Frequency

Flutter

Frequency

Critical speed

Amplitude ratio

Critical frequency parameter.

Fig. 10 refers to tests in which mass was added forward of the leading edge, whilst Fig. 11 refers to the tests with internal mass-loading. Both of these diagrams, and especially Fig. 10 suggest that a rapid change in resonance characteristics is accompanied by a rapid change in flutter characteristics.

For both cases of mass-loading, the frequency of the first type of flutter lies between the first and second resonance frequencies, and for the second type between the second and third resonance frequencies. Also as mass is added, the second resonance nodal line over the outer portion of the wing moves forward and eventually reaches a position ahead of the leading edge ; the corresponding change in the third resonance nodal line entails a movement in towards the wing from the rear, until a position approximately at mid-chord is reached. These movements of the nodal lines, together with the disposition of the flutter frequency in relation to the resonance frequencies, are significant in connection with the so-called Küssner procedure for obtaining a rough estimate of the flutter critical speed. This procedure is dealt with in the next section.

7. *Küssner Criterion.*—Resonance characteristics are determined by elastic and inertial properties and in some respects by damping properties. On the other hand, flutter properties are determined by these same quantities together with the aerodynamic properties. It is therefore clear that resonance tests alone can never yield a precise knowledge of the flutter properties (*e.g.*, an accurate prediction of the critical speed), but based on experience of more or less similar structures they may be used as a guide to the general qualitative flutter characteristics. Küssner

in some very early work[12, 13] put these ideas into a more quantitative form by developing empirically and with some amount of theoretical backing the following relation to give a lower limit to the flutter critical speed :—

$$V_c = Kfc_m$$

where c_m is the mean chord of the oscillating wing,

f is the frequency associated with the ' dangerous resonance.'

For the type of aircraft current at that time (1935), Küssner's work[12] suggested that the value of K (the Küssner coefficient) would lie between 2·8 and 5·4, whilst Pugsley[13] considered values between 3·5 and 6·0. Any resonance that has a nodal line within the region 0·25 to 1·0 chord behind the leading edge is to be classed as ' dangerous,' and the condition most susceptible to flutter, and thus requiring a low value of K is that having a nodal line at 0·75 chord.

A comparison of the diagrams of nodal position with the critical speed as shown in Figs. 10 and 11 suggests, in the light of Küssner's definition of a dangerous resonance, that the first branch of the critical speed curve be associated with a ' dangerous ' second resistance, and the second branch with a ' dangerous ' third resonance. Table 9 gives the values of the Küssner coefficient $K(\equiv V_c/fc_m)$ calculated on this basis from the measured critical speeds and the appropriate resonance frequencies for various conditions of mass-loading. The region $\mu = 0{\cdot}8$ to 0·9 for the internal loading case appears to be anomalous since the nodal positions indicate that the second resonance can hardly be classed as dangerous. A Küssner prediction in this region would suggest that already the first branch of the critical speed curve was tending to infinity, and that the second branch corresponding to the third resonance was now the lower. In other words, the resonance results would suggest an earlier change from the first to the second type of flutter as mass is added. A possible explanation of this apparent discrepancy is that, since the flutter and resonance tests were separated by some months, a change in the elastic properties of the wing (*see* section 4) led to a displacement of the flutter parameters relative to the resonance ones along the μ axis of Fig. 11.

In Küssner's attempt to provide a theoretical correlation between K and the position of the nodal line, the conditions were examined under which energy may be absorbed from the air stream by a two-dimensional aerofoil performing an oscillation in pitching and vertical translation. After an optimum value had been assigned to the phase difference between the two motions, a relation was found between the amplitude ratio and the frequency parameter ω $(\equiv pc/V)$ for the limiting case of zero energy input, which corresponds to the critical flutter condition. The next steps in the correlation were :

(*a*) to identify the flutter amplitude ratio with the dangerous resonance amplitude ratio (*i.e.*, the nodal position),

(*b*) to identify the flutter frequency with the resonance frequency.

Thus a relation between $K \equiv (V_c/fc_m)$ and nodal position was found which is shown in Fig. 12. Steps (*a*) and (*b*) (above) cannot be justified, and the relation between K and nodal position has no strict basis. However, on the basis of vortex-sheet theory air loads, and in the absence of structural damping it is true that as a resonance nodal line approaches the 0·75 chord position the flutter critical speed approaches zero[14]. It would therefore be expected that the variation of critical speed with nodal position for a practical wing would show a minimum at 0·75 chord, which is in qualitative agreement with the relation developed above.

It will be noted that for step (*a*) in the above development to be valid, it would be necessary for the flutter motion of a wing to be identical with that which can be obtained by recombining with a phase difference the separate flexural and torsional displacements at one particular resonance. An assumption of this nature at one time provided a basis for a suggested procedure for critical speed calculation[15].

The experimental results do not justify the theory. The following table shows that the amplitude ratio for the dangerous resonance and flutter are certainly not identical.

Wing condition	Tip amplitude ratio $\Phi\Theta$	
Code letter (*see* Table 8).	Dangerous resonance	Flutter
I_0 (Bare wing)	0·042	0·23
I_1 Internal	0·047	0·26
I_2 mass-loading	0·052	0·32
E_1 External	0	0·41
E_2 mass-loading	0·064	0·10
E_3	0·059	0·10

The theoretical optimum phase displacement for the extraction of energy from an air stream by an oscillating aerofoil[14] is plotted against frequency parameter in Fig. 13. Also included in this diagram are the limiting values of phase displacement outside of which energy cannot be obtained from the stream. The present experimental results referring both to the tip and to the 0·7 span section are also plotted on the diagram and it is seen that they do lie within the region of absorption, but that they do not fall on the curve of optimum phase.

In Fig. 12 the experimental values of K and the positions of the nodal lines taken from Table 9 are plotted so that each systematic series of results appears as a line. The only other results of this nature known to the writer are those of Jones and Scruton[4] which are included in the diagram. In spite of the fact that the derivation of the theoretical relation is not justified, the experimental values fall reasonably close to the theoretical curve, but it is unfortunate that the nodal positions do not cover a wider range.

8. *Conclusions regarding Correlation between Resonance and Flutter Characteristics.*—Although it would seem impossible to obtain a strict correlation between critical speed and resonance characteristics, a non-dimensional parameter of the Küssner type clearly allows a comparison to be made of the critical speeds of sets of wings showing dynamical similarity. Even when strict dynamical similarity does not exist, a parameter of this type may be of use in transferring experience gained from one system to another. Gradually, as the results of resonance and model flutter tests accumulate, it should be possible to build up a body of experience by which flutter qualities may be judged from resonance tests.

9. *Analysis of Flutter Nodes into Normal Modes.*—9.1. *Method of analysis.*—The wing distortion corresponding to the rth normal mode of oscillation may be defined in terms of flexure and torsion as follows :

$$\Phi_r = \bar{\Phi}_r f_r(\eta) \quad \ldots \quad (1)$$

$$\Theta_r = \bar{\Theta}_r F_r(\eta) \quad \ldots \quad (2)$$

$$\bar{\Phi}_r/\bar{\Theta}_r = -\bar{X}_r/s \quad \ldots \quad (3)$$

where Φ_r and Θ_r are respectively flexural and torsional amplitudes, the barred terms referring to a conveniently chosen reference section*, and $\bar{X}_r$ is the distance aft of the OY axis of the node at the reference section. Since the motions are either in phase or in opposition, no restriction need be placed on the sign of the amplitudes.

* It is assumed that the reference section is chosen so that $f(\eta)$ and $F(\eta)$ are in general finite. In the numerical and experimental work the reference section was taken at the tip.

Substitution of Φ_r from equation (3) in equation (1) allows the mode to be defined in terms of a sole arbitrary amplitude $\bar{\Theta}_r$ as follows :—

$$\Phi_r = -(\bar{X}_r/s)\bar{\Theta}_r f_r(\eta) \quad .. \quad .. \quad .. \quad .. \quad .. \quad .. \quad .. \quad (4)$$

$$\Theta_r = \bar{\Theta}_r F_r(\eta). \quad .. \quad .. \quad .. \quad .. \quad .. \quad .. \quad .. \quad .. \quad (5)$$

The wing motion during a steady flutter oscillation of circular frequency p may be specified in terms of flexure and torsion as follows :—

$$\phi_F = \Phi_F \sin [pt + \alpha(\eta)] = \bar{\Phi}_F f_F(\eta) \sin [pt + \alpha(\eta)] \quad .. \quad .. \quad .. \quad (6)$$

$$\theta_F = \Theta_F \sin [pt + \beta(\eta)] = \bar{\Theta}_F F_F(\eta) \sin [pt + \beta(\eta)] \quad .. \quad .. \quad .. \quad (7)$$

$$\bar{\Phi}_F/\bar{\Theta}_F = -X_F/s\,. \quad .. \quad .. \quad .. \quad .. \quad .. \quad (8)$$

Since in general phase differences are present during flutter, amplitudes $\bar{\Phi}_F$, $\bar{\Theta}_F$, and amplitude modes $f_F(\eta)$, $F_F(\eta)$ will be restricted to positive quantities. Furthermore, since nodes do not exist during flutter $\bar{X}_F$ will not have the direct physical significance of a nodal position.

Again the motion can alternatively be specified by the following two relations involving the sole arbitrary amplitude $\bar{\Theta}_F$:—

$$\phi_F = -(\bar{X}_F/s)\bar{\Theta}_F f_F(\eta) \sin [pt + \alpha(\eta)] \quad .. \quad .. \quad .. \quad .. \quad .. \quad (9)$$

$$\theta_F = \bar{\Theta}_F F_F(\eta) \sin [pt + \beta(\eta)]. \quad .. \quad .. \quad .. \quad .. \quad .. \quad .. \quad (10)$$

If the distortion during flutter is regarded as composed of the first n normal mode distortions the following equations hold :—

$$-(\bar{X}_F/s)\bar{\Theta}_F f_F(\eta) \sin [pt + \alpha(\eta)] = \phi$$
$$= \Sigma_1^n -(\bar{X}_r/s)\,\bar{\Theta}_r f_r(\eta) \sin (pt + \varepsilon_r) + \Phi_E \sin [pt + \alpha_E(\eta)] \quad .. \quad .. \quad (11)$$

$$\bar{\Theta}_F F_F(\eta) \sin [pt + \beta(\eta)] = \theta$$
$$= \Sigma_1^n \bar{\Theta}_r F_r(\eta) \sin (pt + \varepsilon_r) + \Theta_E \sin [pt + \beta_E(\eta)] \quad .. \quad .. \quad .. \quad (12)$$

where ε_r is the phase displacement associated with the rth mode. The second terms on the right-hand sides represent the errors in the assumption that the flutter mode can be resolved into the first n normal modes, and will be termed the residual modes.

By a consideration of the in-phase and the out-of-phase components, and with some rearrangement four equations are obtained :—

$$-(\bar{X}_F/s)f_F(\eta) \cos \alpha(\eta) = \Sigma_1^n -(\bar{X}_r/s)f_r(\eta)A_r + (\Phi_E/\bar{\Phi}_F) \cos \alpha_E(\eta) \quad .. \quad (13)$$

$$F_F(\eta) \cos \beta(\eta) = \Sigma_1^n F_r(\eta)A_r + (\Theta_E/\bar{\Theta}_F) \cos \beta_E(\eta) \quad .. \quad .. \quad (14)$$

$$-(\bar{X}_F/s)f_F(\eta) \sin \alpha(\eta) = \Sigma_1^n -(\bar{X}_r/s)f_r(\eta)B_r + (\Phi_E/\bar{\Phi}_E) \sin \alpha_E(\eta) \quad .. \quad (15)$$

$$F_F(\eta) \sin \beta(\eta) = \Sigma_1^n F_r(\eta)B_r + (\Theta_E/\bar{\Theta}_F) \sin \beta_E(\eta) \quad .. \quad .. \quad (16)$$

where

$$\frac{\bar{\Theta}_r}{\bar{\Theta}_F} \cos \varepsilon_r = A_r \quad .. \quad .. \quad .. \quad .. \quad .. \quad .. \quad (17)$$

$$\frac{\bar{\Theta}_r}{\bar{\Theta}_F} \sin \varepsilon_r = B_r. \quad .. \quad .. \quad .. \quad .. \quad .. \quad .. \quad (18)$$

Equations (13) to (16) (above) are true for all values of η. Values of the left-hand side of these equations were available for eight values of η since measurements of the flutter motion had been made at this number of stations (*see* Ref. 7). Corresponding values obtained from measurements of the first four resonances were inserted in the right-hand sides. In this way sixteen equations in A_1, $A_2 \ldots A_4$ and sixteen equations in B_1, $B_2 \ldots B_4$ were obtained. After dividing sets of

equations represented by equations (13) and (15) (above) by $(\bar{X}_F/s)$ to bring the coefficients to the same order as those of sets represented by (14) and (16), a ' least squares ' process was used to obtain values of $A_1, A_2 \ldots A_4$ and $B_1, B_2 \ldots B_4$ and thus the values of $\bar{\Theta}_r/\bar{\Theta}_F$ and ε_r. It was convenient to set the arbitrary amplitude $\bar{\Theta}_F$ at unity, and thus the normal mode components at any spanwise station were then obtained from the relations

$$\Phi_r = -(\bar{X}_r/s)(A_r^2 + B_r^2)^{1/2} f_r(\eta)$$
$$\Theta_r = (A_r^2 + B_r^2)^{1/2} F_r(\eta) .$$

9.2. *Results and Discussions.*—Flutter motions were measured for the six conditions of the wing as specified in Table 8. Resonance data covering the first four modes were obtained for a range of mass-loadings (*see* Ref. 8), and values corresponding to the same conditions were obtained by interpolation. From the values of $A_1, A_2 \ldots A_4$, $B_1, B_2 \ldots B_4$ and $\varepsilon_1, \varepsilon_2 \ldots \varepsilon_4$ obtained in the analyses Figs. 14 to 19 have been prepared to show for each condition the resolution of the flutter distortions into normal mode distortions. These diagrams show the spanwise variations of 5Φ and Θ together with indications of the phase, the amplitudes being regarded as positive throughout. The amplitudes of the residual modes are also included in the diagrams.

It might be expected that there would be a tendency for a normal mode whose associated frequency is close to the flutter frequency to feature prominently in the flutter motions. To illustrate any such tendency, values of the ratio (f_r/f_F) are included in the diagrams.

Each loading condition will now be dealt with separately.

I_0 (*Bare wing*) : *Fig.* 14.—As is to be expected, the flutter mode can be regarded as a combination of the first two normal modes alone. The other modes provide negligible components.

I_1 : *Fig.* 15.—A concentrated mass of more than twice the mass of the wing has been added internally, but the second branch of the critical speed curve has not been reached (*see* Fig. 11c). Each of the first three modes enter into the flutter mode.

I_2 : *Fig.* 16.—This condition also refers to the internal addition of a mass more than twice the mass of the wing, but now the second branch of the critical speed curve has been reached. The fourth mode now enters into the flutter motion although not to a great extent, and it is conceivable that its omission might not appreciably alter the calculated critical speed.

E_1 : *Fig.* 17.—Here an external concentrated mass of nearly half the mass of the wing has been added (*see* Fig. 10c). The first three modes contribute components, but it is possible that a good estimate of the critical speed might be obtained using only the first two.

E_2 : *Fig.* 18.—The second branch of the critical speed curve has now been reached. The first three modes are necessary to define the flutter mode accurately, but it is possible that a calculation based on the first and third only might yield a reasonably accurate critical speed.

E_3 : *Fig.* 19.—A further addition of mass has been made. As with E_2 the first three modes enter into the flutter mode, but it might be sufficiently accurate to include only the first and the third.

9.3. *General Conclusions regarding Analysis of Flutter Modes.*—In only one of the six cases analysed does the fourth mode feature to any appreciable extent, and even here it is probable that its presence would not be necessary for a reasonable estimate of the critical speed. The results suggest that the first three normal modes of wing motion should be sufficient for calculation purposes, but it must be remembered that this is on the assumption of the absence of bodily freedoms.

10. *Acknowledgement.*—Acknowledgement is made to Mrs. C. H. Wilkinson for her assistance in the computational work involved in this report.

LIST OF SYMBOLS

OX	Chordwise axis } *see* Fig. 1
OY	Spanwise axis } *see* Fig. 1
s	Span
c	Chord
c_m	Mean chord
η	Spanwise co-ordinate $\equiv y/s$
z	Normal displacement at reference axis OY
$\mathscr{A}(\eta\eta')$	Flexibility coefficients (*see* section 3)
$\mathscr{B}(\eta\eta')$	
$\mathscr{C}(\eta\eta')$	
$\mathscr{D}(\eta\eta')$	
ϕ	Flexural displacement $\equiv z/s$ } *see* Fig. 1
θ	Torsional displacement } *see* Fig. 1
Φ, Θ	Amplitudes of ϕ and θ respectively
$\bar{\Phi}$, $\bar{\Theta}$	Values of Φ and Θ respectively appropriate to a reference section
$f(\eta)$	Mode of flexural distortion $\equiv \Phi/\bar{\Phi}$
$F(\eta)$	Mode of torsional distortion $\equiv \Theta/\bar{\Theta}$
X	$-s(\Phi/\Theta)$ (for resonances, the node is distance X behind the OY-axis)
$\bar{X}$	Value of X at reference section
p	Circular frequency (radians/sec)
$f \equiv$	$p/2\pi$, frequency (cycles/sec)
f_c, f_F	Flutter frequency
V	Air speed
V_c	Critical air speed for flutter
ω	Frequency parameter $\equiv (pc/V)$
K	Küssner coefficient $\equiv (V_c/fc_m)$
ε, ξ	Phase angles
$\alpha(\eta)$	Flexural phase angle at station η
$\beta(\eta)$	Torsional phase angle at station η
A	*see* equations (17) and (18)
B	*see* equations (17) and (18)
μ	Added mass in slugs

Suffices

r	Refers to the rth normal mode
F	Refers to the flutter condition
E	Refers to a residual distortion

REFERENCES

No.	*Author*	*Title, etc.*
1	A. G. Pugsley	Resonance tests, their history and principles in relation to flutter theory. *Aircraft Engineering*. March, 1938.
2	P. B. Walker and A. W. Clegg	The technique of wing resonance tests. R. & M. 2046. February, 1939.
3	W. G. Molyneux and E. G. Broadbent	Ground resonance testing of aircraft. R. & M. 2155. July, 1946.
4	W. P. Jones and C. Scruton	Flutter and resonance tests of a flexible model wing with special reference to Küssner's formula. A.R.C. 2392. 1936. (Unpublished.)
5	J. Hanson and E. Warlow-Davies ..	Model experiments on the effect of wing engines on the natural frequencies and modes of vibration of wings. R. & M. 2128. April, 1939.
6	J. Taylor	Further model experiments on the effect of wing engines on the natural frequencies of modes of vibration of wings. R. & M. 2128. April, 1939.
7	N. C. Lambourne and D. Weston ..	An experimental investigation of the effect of localised masses on the flutter of a model wing. R. & M. 2533. April 1944.
8	N. C. Lambourne and D. Weston ..	An experimental investigation of the effect of localised masses on the flutter and resonances of a model wing. Part II. Resonance and stiffness tests. A.R.C. 11,008. November, 1947.
9	R. A. Frazer	Interim note on a theoretical investigation of the influence of mass on wing flutter. A.R.C. 6720. 1943. (Unpublished.)
10	R. A. Frazer	Addendum to Interim Note 6720 ' On a theoretical investigation of the influence of mass on wing flutter.' A.R.C. 6833. 1943. (Unpublished.)
11	A. A. Griffiths and C. Wigley	A preliminary investigation of certain elastic properties of wood. R. & M. 528. February, 1919.
12	H. G. Küssner	The present stage of development of the problem of wing flutter. *L.F.F.* Vol. 12, p. 193. October, 1935.
13	A. G. Pugsley	Preliminary note on Küssner's flutter speed formula. R.A.E. Report A.D. 3074. A.R.C. 2415. 1936. (Unpublished.)
14	N. C. Lambourne	On the conditions under which energy can be extracted from an air stream by an oscillating aerofoil. A.R.C. 12,213. March, 1949. (*Aero. Quart.*, Vol. IV, p. 54. August, 1952.)
15	A. G. Pugsley	Note on some R.A.E. work on the estimation of wing flutter speeds from resonance test results. R.A.E. Report A.D. 3130. A.R.C. 4298. 1939. (Unpublished.)

TABLE 1

Inertial Constants of Bare Wing

η	Rib	Mass (slugs)	Mass moment about y-axis* (slugs ft)	Intertia about y-axis* (slugs ft^2)
	1	0·00995	0·00264	0·00543
	2	0·00887	0·00232	0·00499
0·1	3	0·05610	0·01440	0·03332
	4	0·00832	0·00210	0·00439
	5	0·00783	0·00195	0·00468
0·2	6	0·03929	0·00960	0·01644
	7	0·00766	0·00183	0·00370
	8	0·00736	0·00173	0·00349
0·3	9	0·03639	0·00842	0·01509
	10	0·00724	0·00165	0·00316
	11	0·00694	0·00155	0·00291
0·4	12	0·02779	0·00607	0·00956
	13	0·00667	0·00143	0·00260
	14	0·00642	0·00135	0·00234
0·5	15	0·03129	0·00644	0·01056
	16	0·00598	0·00121	0·00204
	17	0·00602	0·00119	0·00198
0·6	18	0·02123	0·00406	0·00576
	19	0·00516	0·000972	0·00159
	20	0·00510	0·000939	0·00155
0·7	21	0·02024	0·003643	0·00481
	22	0·00480	0·000844	0·01339
	23	0·00463	0·000793	0·00123
0·8	24	0·01708	0·002852	0·00350
	25	0·00424	0·000690	0·00103
	26	0·00410	0·000650	0·000955
0·9	27	0·01374	0·002118	0·002459
	28	0·00368	0·000560	0·000777
	29	0·00344	0·000501	0·000704
1·0	30	0·00681	0·001046	0·001258

Total Weight of Bare Wing = 12·7 lb ($\equiv$ 0·394 slug).

*The y-axis is perpendicular to the wing root and situated at 0·3c from the leading edge (*see* Fig. 1).

TABLE 2

Additional Inertias for Engine Mass Mountings (including the Streamlined Cases)

	Mass (slugs)	Mass moment about y-axis (slugs ft)	Inertia about y-axis (slugs ft^2)
Engine Mounting at η = 0·1	0·0849	−0·0922	0·1035
,, ,, ,, η = 0·3	0·0808	−0·0757$_5$	0·0793
,, ,, ,, η = 0·5	0·0774	−0·0634	0·0593

TABLES 3, 4 and 5

Standard Set of Flexibility Coefficients

$\mathscr{A}(\eta\eta')$ = flexure at η due to unit force at η'.

$\mathscr{B}(\eta\eta')$ = flexure at η due to unit couple at η'.

$\mathscr{C}(\eta\eta')$ = twist at η due to unit couple at η'.

$\mathscr{D}(\eta\eta')$ = twist at η due to unit force at η'.

TABLE 3

$\mathscr{A}(\eta\eta') \times 10^3$ (ft, lb^{-1})

		η'									
		0·1	0·2	0·3	0·4	0·5	0·6	0·7	0·8	0·9	1·0
η	0·1	0·061	0·084	0·133	0·151	0·180	0·201	0·250	0·251	0·279	0·339
	0·2		0·240	0·380	0·479	0·584	0·667	0·771	0·870	0·984	1·07
	0·3			0·670	0·950	1·19	1·45	1·71	1·96	2·20	2·48
	0·4				1·50	2·05	2·52	3·05	3·53	4·08	4·57
	0·5					2·94	3·87	4·81	5·77	6·71	7·67
	0·6						5·41	7·06	8·66	10·3	11·9
	0·7							9·67	12·2	14·9	17·5
	0·8								16·3	20·3	24·4
	0·9									26·2	32·1
	1·0										40·4

TABLE 4

$\mathscr{C}(\eta\eta') \times 10^3$ (ft^{-1}, lb^{-1})

		η'									
		0·1	0·2	0·3	0·4	0·5	0·6	0·7	0·8	0·9	1·0
η	0·1	0·082	0·146	0·196	0·225	0·232	0·242	0·264	0·264	0·278	0·273
	0·2		0·386	0·581	0·717	0·806	0·872	0·900	0·907	1·02	0·996
	0·3			1·06	1·39	1·64	1·84	1·93	2·01	2·13	2·14
	0·4				2·09	2·66	3·11	3·34	3·59	3·81	3·92
	0·5					3·76	4·62	5·27	5·70	6·09	6·37
	0·6						6·28	7·64	8·71	9·50	10·0
	0·7							10·2	12·5	14·1	15·1
	0·8								16·5	19·8	22·0
	0·9									25·4	29·5
	1·0										36·4

TABLE 5

$\mathscr{B}(\eta\eta') \times 10^3 = \mathscr{D}(\eta'\eta) \times 10^3$ (lb^{-1})

		η'									
		0·1	0·2	0·3	0·4	0·5	0·6	0·7	0·8	0·9	1·0
η	0·1	−0·006	−0·010	−0·010	−0·015	−0·020	−0·030	−0·035	−0·040	−0·035	−0·035
	0·2	−0·008	−0·015	−0·020	−0·040	−0·050	−0·070	−0·075	−0·100	−0·120	−0·115
	0·3	−0·015	−0·035	−0·050	−0·080	−0·105	−0·135	−0·155	−0·180	−0·185	−0·170
	0·4	−0·020	−0·050	−0·080	−0·110	−0·150	−0·185	−0·235	−0·280	−0·280	−0·265
	0·5	−0·035	−0·080	−0·120	−0·185	−0·220	−0·255	−0·320	−0·365	−0·370	−0·370
	0·6	−0·040	−0·115	−0·170	−0·265	−0·310	−0·360	−0·420	−0·455	−0·430	−0·435
	0·7	−0·060	−0·145	−0·230	−0·340	−0·425	−0·470	−0·505	−0·495	−0·455	−0·450
	0·8	−0·065	−0·165	−0·280	−0·415	−0·525	−0·635	−0·605	−0·490	−0·450	−0·505
	0·9	−0·085	−0·190	−0·330	−0·490	−0·650	−0·810	−0·780	−0·640	−0·510	−0·300
	1·0	−0·085	−0·215	−0·395	−0·580	−0·790	−1·025	−1·025	−0·820	−0·545	−0·245

TABLE 6

Position of Flexural Centre

η	Distance aft of leading edge as ratio of local chord
0·1	0·33
0·2	0·32
0·3	0·32
0·4	0·32
0·5	0·33
0·6	0·33
0·7	0·33
0·8	0·32
0·9	0·31
1·0	0·30

TABLE 7

Change of Elastic Characteristics of Wing

	Stiffnesses*		Flutter characteristics of bare wing	
	l_ϕ (lb ft/radn)	m_θ (lb ft/radn)	V_c (ft/sec)	f_c (cycles/sec)
1942 March/April (Completion of standard flexibility coefficient measurements)	1790	97·8		
1942 October (Completion of preliminary resonance tests)	1754	88·0		
1942 December (Commencement of flutter tests)			86·1	5·45
1943 January (After repair to wing)	1838	94·9	88·2	5·55
1943 March			89·3 90·0	5·5 5·45
1943 April			89·3 89·4	5·45 —
1943 May			89·2	5·4
1943 July			88·8 88·6	5·12 5·18
1943 August (Completion of flutter tests)	1550	85·3		
1944 May (Commencement of main resonance tests)	1738	90·4		
1944 August (Completion of main resonance tests)	1680	89·4		

* Flexural stiffness $l_\phi = 0{\cdot}49s^2W/z$ where z is the displacement at $\eta = 0{\cdot}7$ due to a load W applied at the flexural centre at $\eta = 0{\cdot}7$.

Torsional stiffness $m_0 = M/\theta$ where θ is the torsional displacement at $\eta = 0{\cdot}7$ due to a couple M applied at $\eta = 0{\cdot}7$.

TABLE 8

The Wing Conditions for which the Flutter Motions were Analysed (see also Figs. 10c and 11c)

Code letter	Condition	
I_0	Bare wing	
I_1	Internal loading ($\eta = 0{\cdot}3$, $0{\cdot}3c$ aft leading edge)	$\mu = 0{\cdot}87$ slugs
I_2	,,	$\mu = 0{\cdot}94$
E_1	External loading ($\eta = 0{\cdot}3$, $0{\cdot}28c$ forward leading edge	$\mu = 0{\cdot}17$
E_2	,,	$\mu = 0{\cdot}24$
E_3	,,	$\mu = 0{\cdot}32$

TABLE 9

Mass-loading condition	Critical speed V_c	Dangerous resonance	Resonance frequency	Küssner coefficient Vc/fc_m	Position of nodal line in chords behind leading edge	
					Tip section	0·7 span
External mass-loading						
	ft/sec		cycles/sec			
(a) $\mu = 0$ slug	95	2nd	6·7	6·9	0·44	0·40
0·1	105	,,	5·8	8·8	0·37	0·37
(b) 0·15	115	,,	5·5	10·15	0·32	0·34
— —	—	—	—	—	—	—
(c) 0·2	123	3rd	9·0	6·7	0·58	0·38
0·3	114	,,	8·75	6·3	0·55	0·39
0·4	108	,,	8·5	6·2	0·54	0·40
0·5	105	,,	8·5	6·0	0·54	0·40
1·0	100	,,	8·5	5·7	0·53	0·40
1·5	98	,,	8·5	5·6	0·53	0·40
2·0	97	,,	8·5	5·6	0·53	0·40
(d) ∞	97	,,	8·5	5·6	0·52	0·40
Internal mass-loading						
(e) $\mu = 0$ slug	90	2nd	7·25	6·0	0·48	0·40
0·2	92	,,	7·25	6·2	0·48	0·42
0·4	94·5	,,	7·2	6·4	0·44	0·42
0·6	97·5	,,	7·0	6·8	0·33	0·39
0·8	102	,,	6·5	7·6	0·14	0·33
(f) 0·9	104	,,	6·3	8·0	0·02	0·29
— —	—	—	—	—	—	—
(g) 0·95	95	3rd	7·3	6·3	0·52	0·42
1·0	88	,,	7·25	5·9	0·52	0·42
1·1	83	,,	7·25	5·6	0·52	0·41
1·3	80	,,	7·25	5·4	0·52	0·41
1·5	79	,,	7·25	5·3	0·52	0·41
1·7	79	,,	7·25	5·3	0·52	0·41
1·9	80	,,	7·25	5·4	0·52	0·41
2·2	81	,,	7·25	5·4	0·52	0·41
(h) ∞	84	,,	7·2	5·5	0·52	0·41

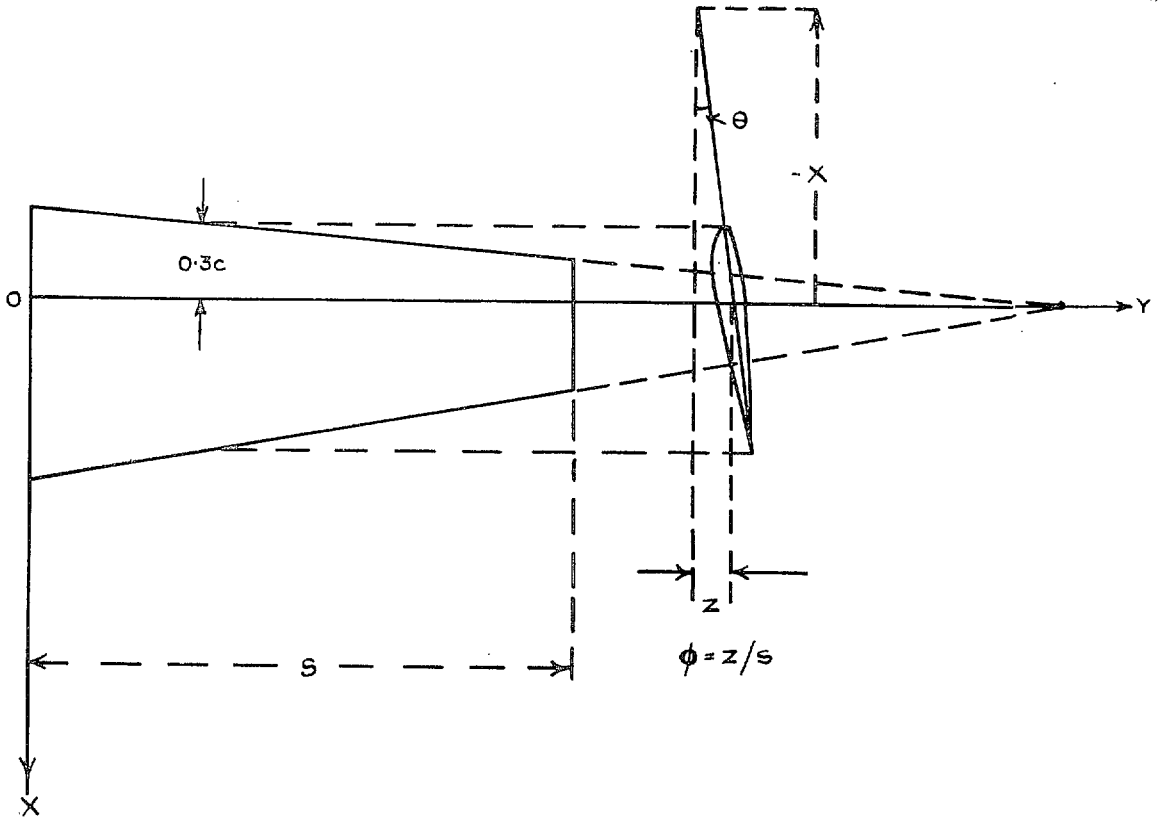

FIG. 1. Definitions.

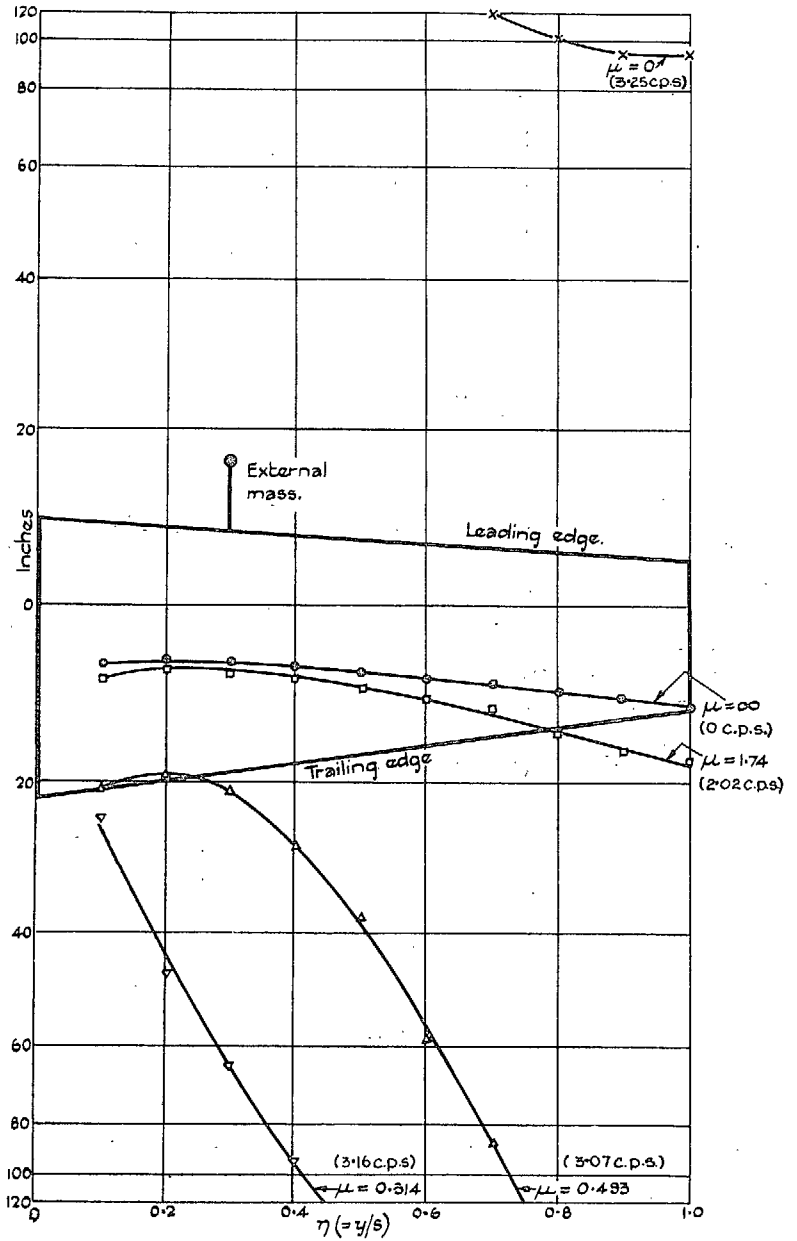

FIG. 2. Nodal lines for 1st resonances. External mass-loading (μ in slugs).

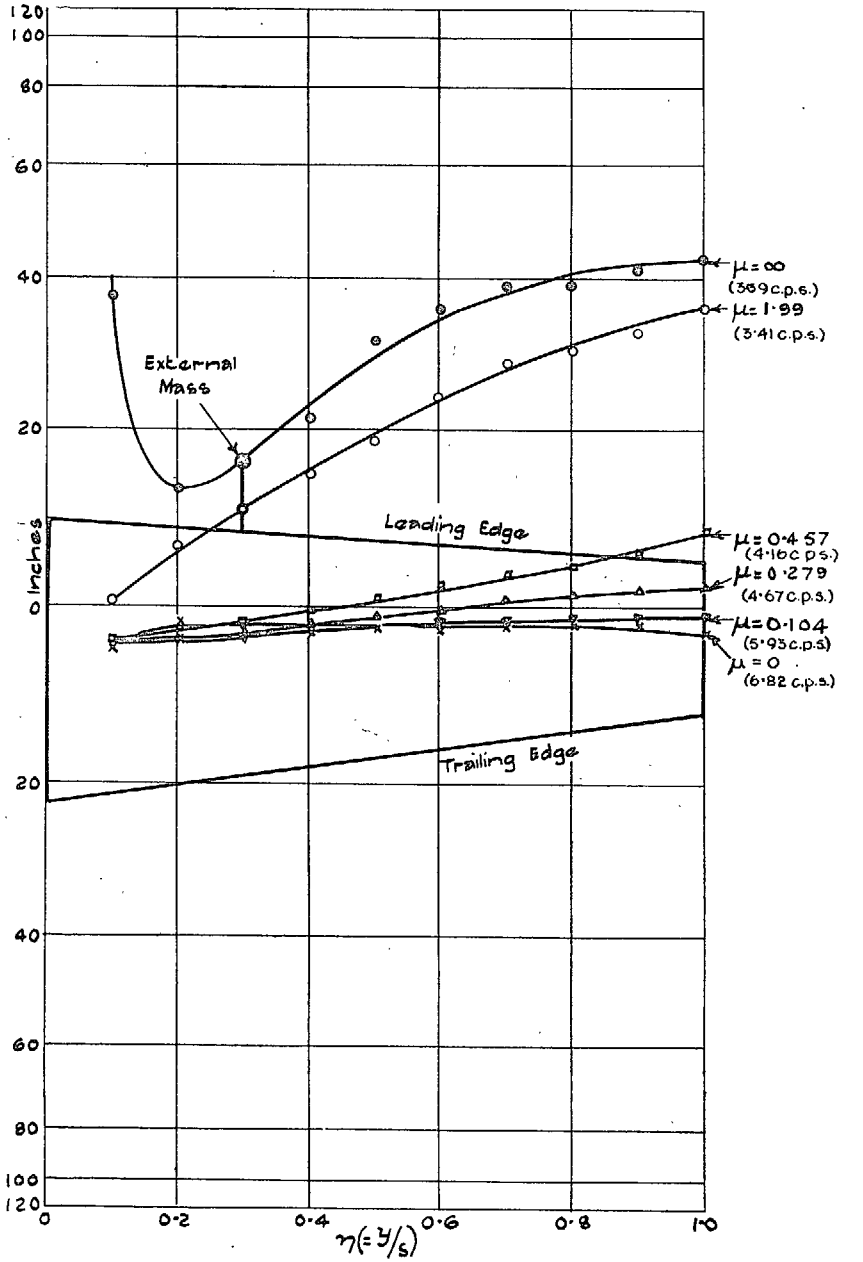

FIG. 3. Nodal lines for 2nd resonances. External mass-loading (μ in slugs).

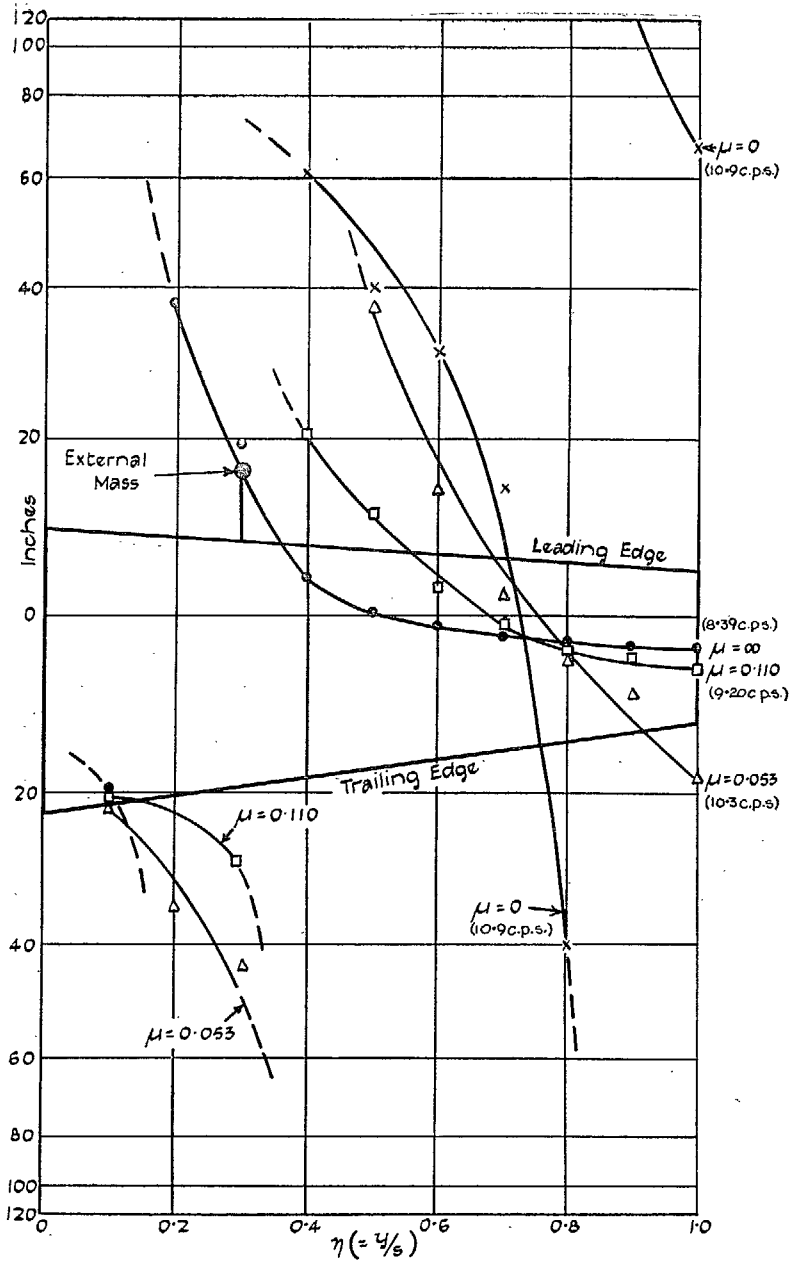

FIG. 4. Nodal lines for 3rd resonances. External mass-loading (μ in slugs).

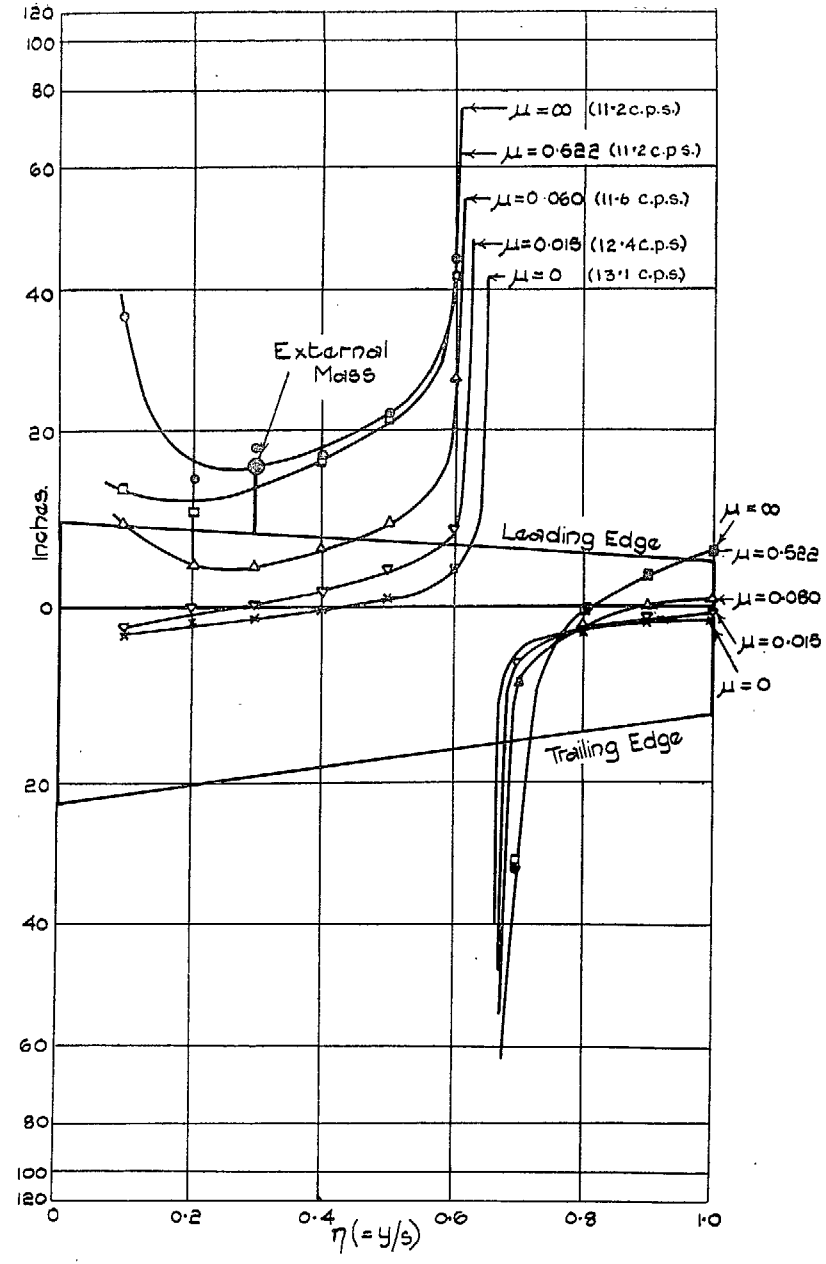

FIG. 5. Nodal lines for 4th resonances. External mass-loading (μ in slugs).

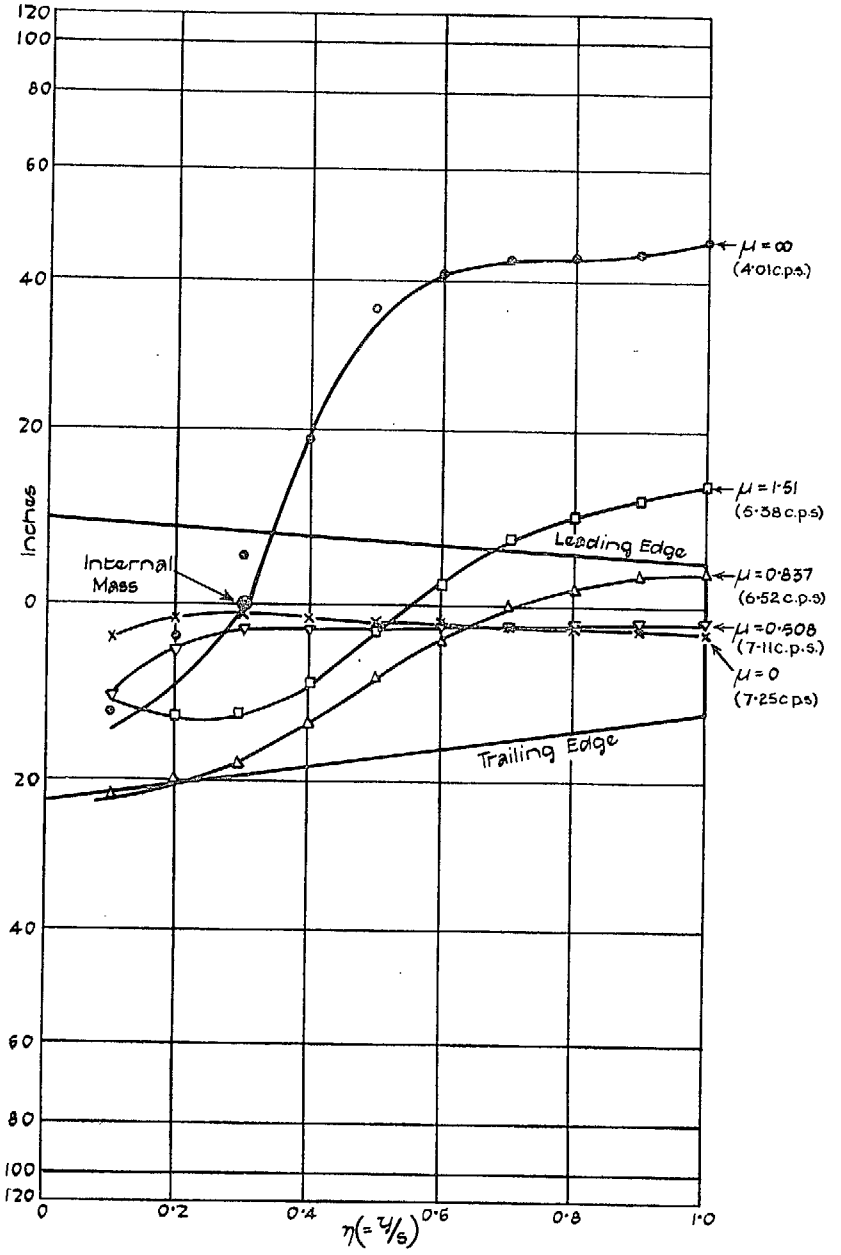

FIG. 6. Nodal lines for 2nd resonances. Internal mass-loading (μ in slugs).

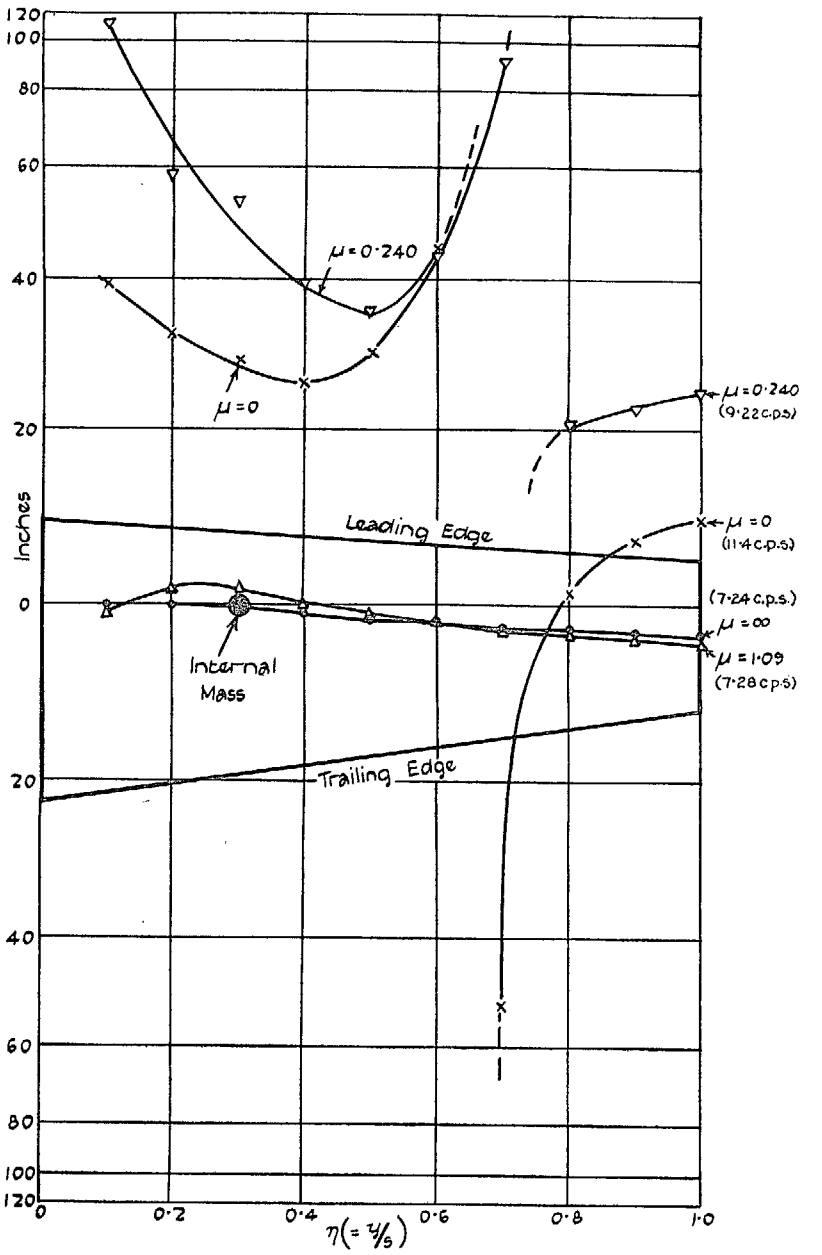

FIG. 7. Nodal lines for 3rd resonances. Internal mass-loading (μ in slugs).

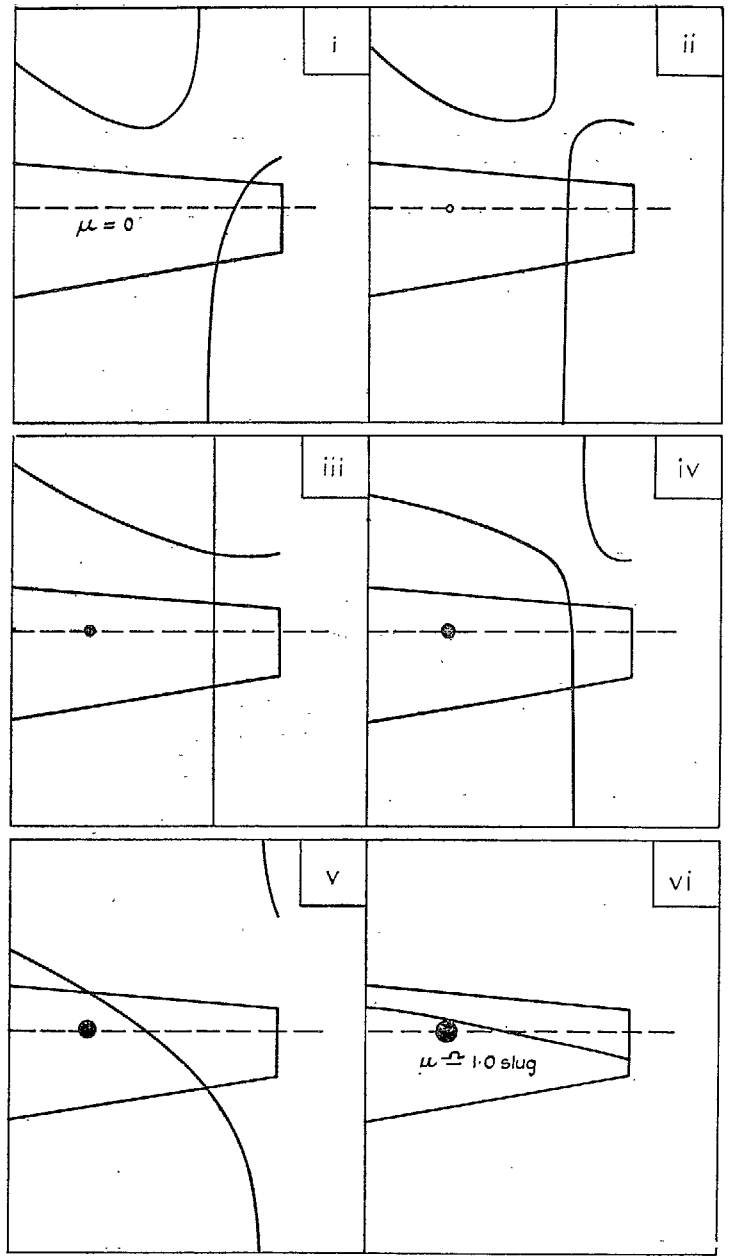

FIG. 8. Probable sequence of nodal lines for 3rd resonance. Internal mass-loading.

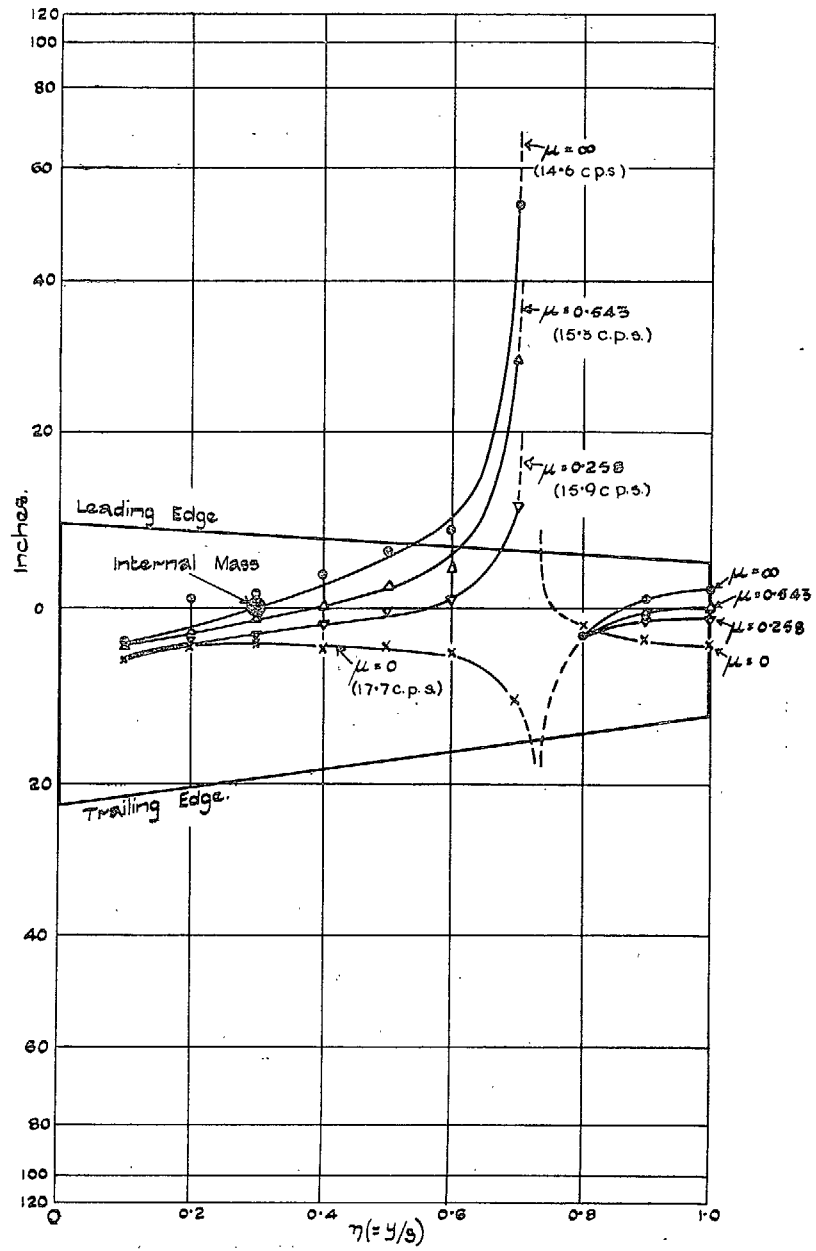

FIG. 9. Nodal lines for 4th resonances. Internal mass-loading (μ in slugs).

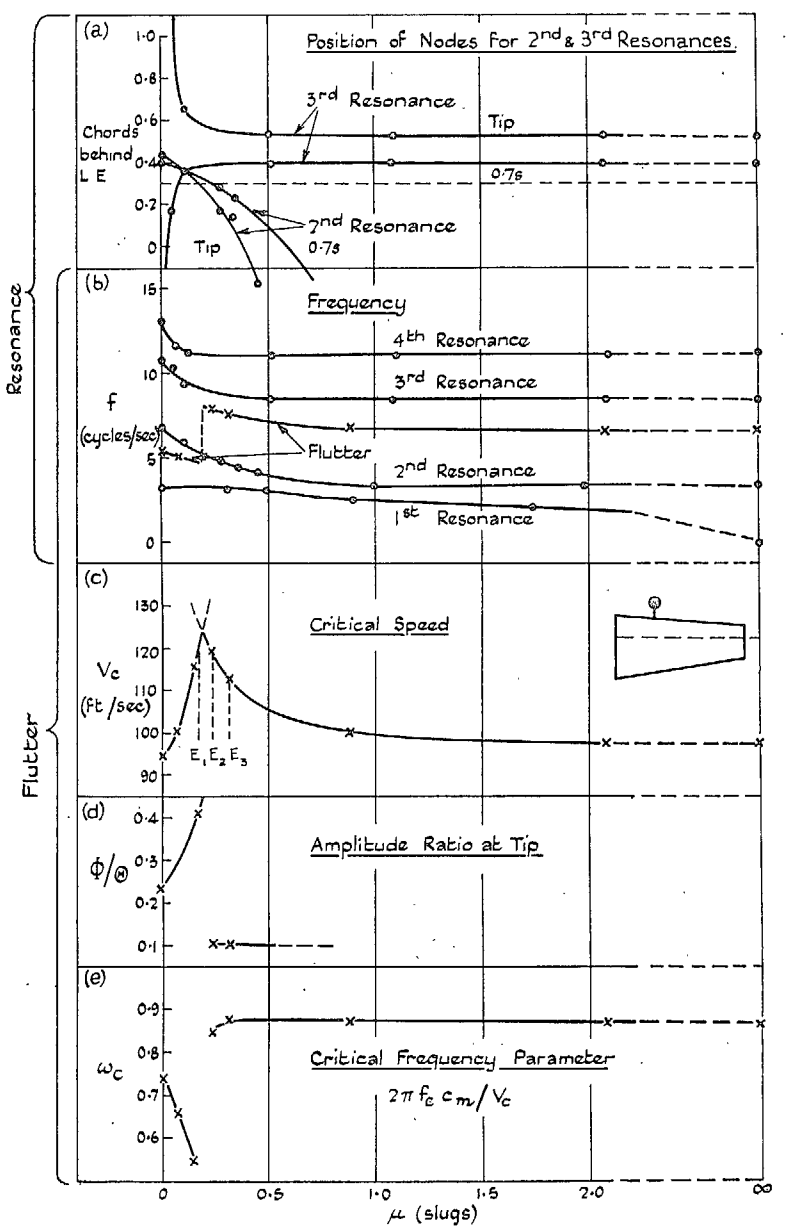

FIG. 10. Variation of resonance and flutter characteristics with external mass.

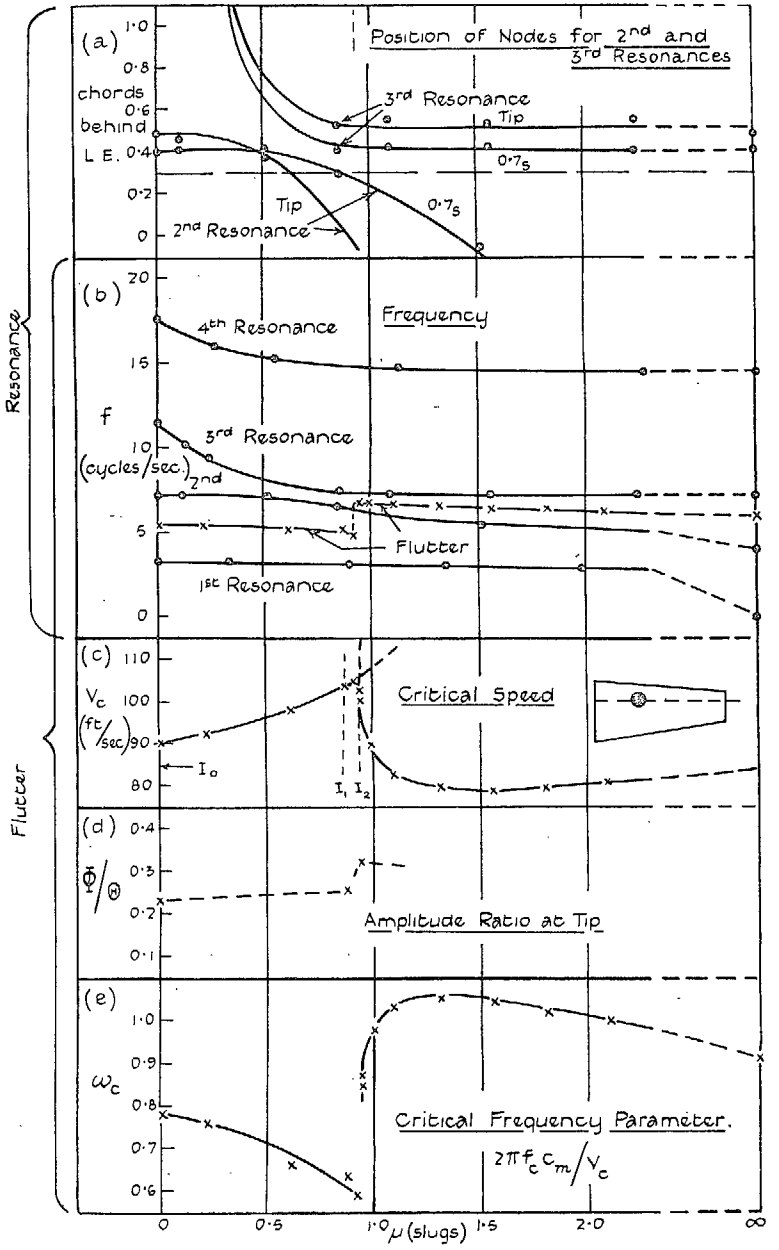

FIG. 11. Variation of resonance and flutter characteristics with internal mass.

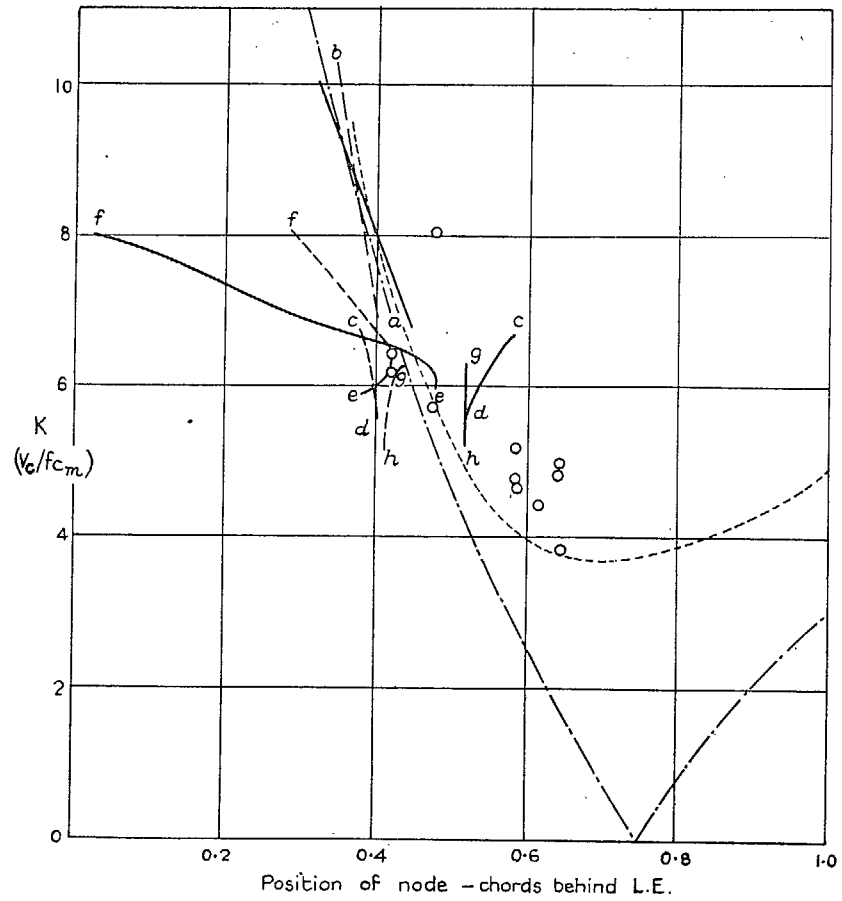

FIG. 12. Küssner coefficient K and position of node at the ' dangerous ' resonance.

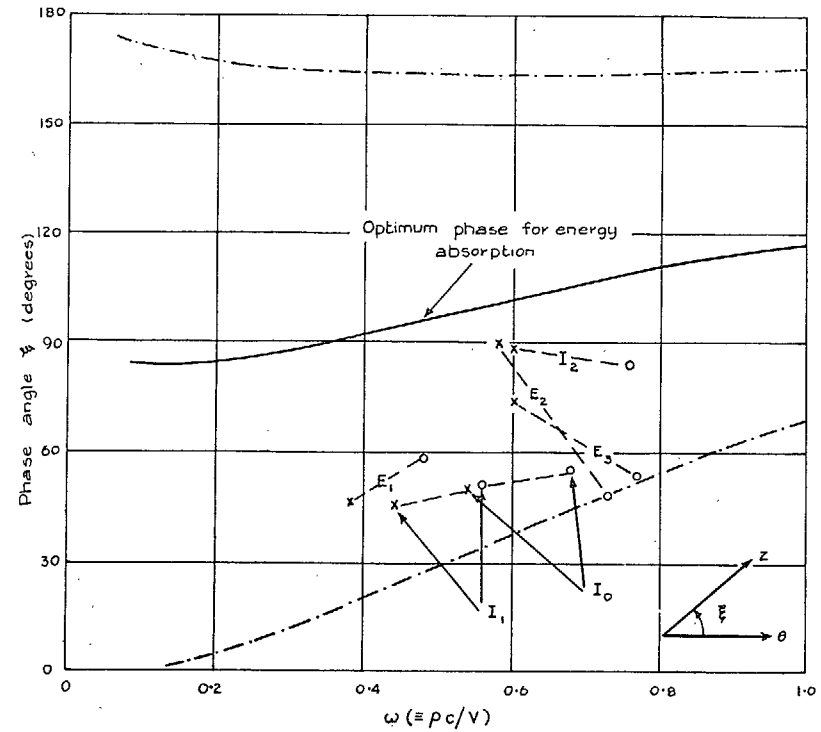

[ξ is the angle by which vertical translation (or flexure) leads pitching (or torsion)] Theoretical boundaries of energy absorption region for two-dimensional pitching and vertical translation are denoted by
Experimental values from flutter tests are shown by:-
x refering to tip section } code letters refer to wing
o refering to 0·7s section } conditions as given in table 8.

FIG. 13. Variation of phase difference ξ with frequency parameter ω for flutter.

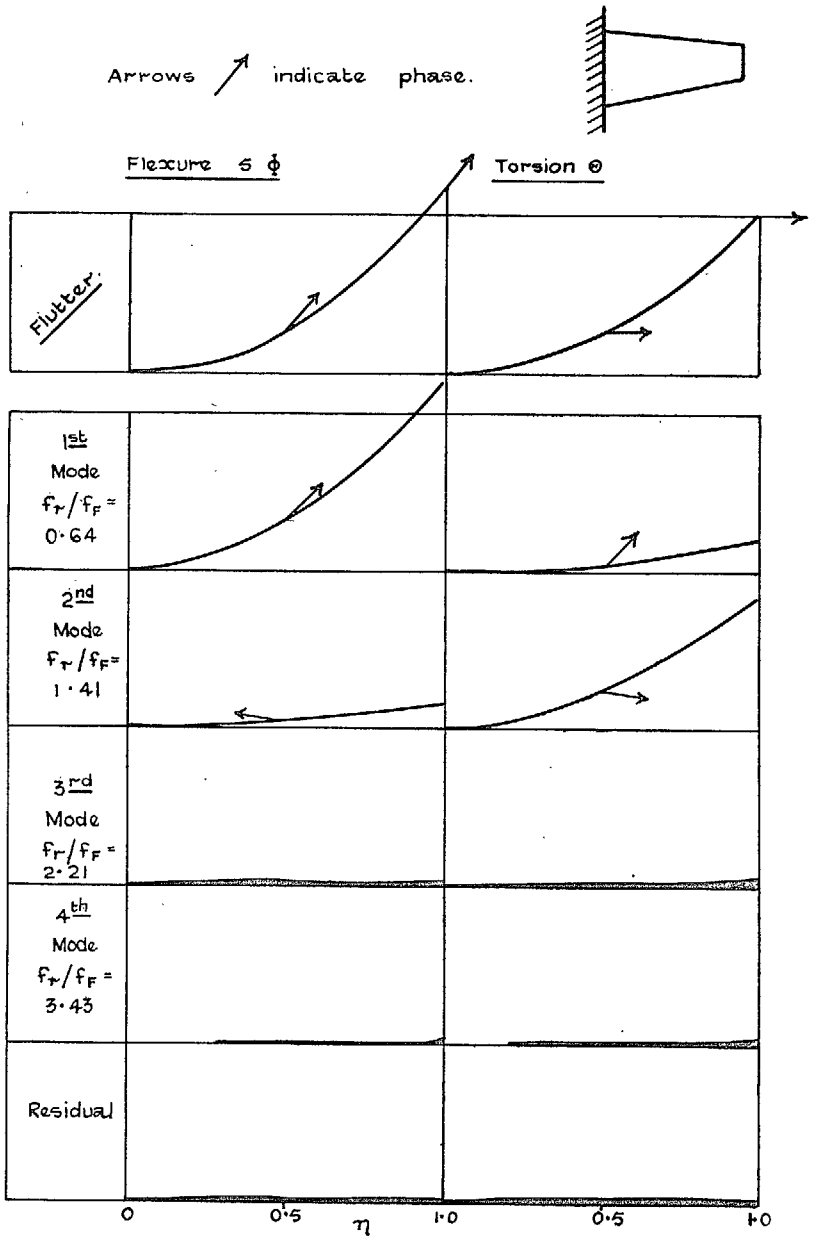

FIG. 14. Flutter mode resolved into normal mode components. Bare wing (condition I_0).

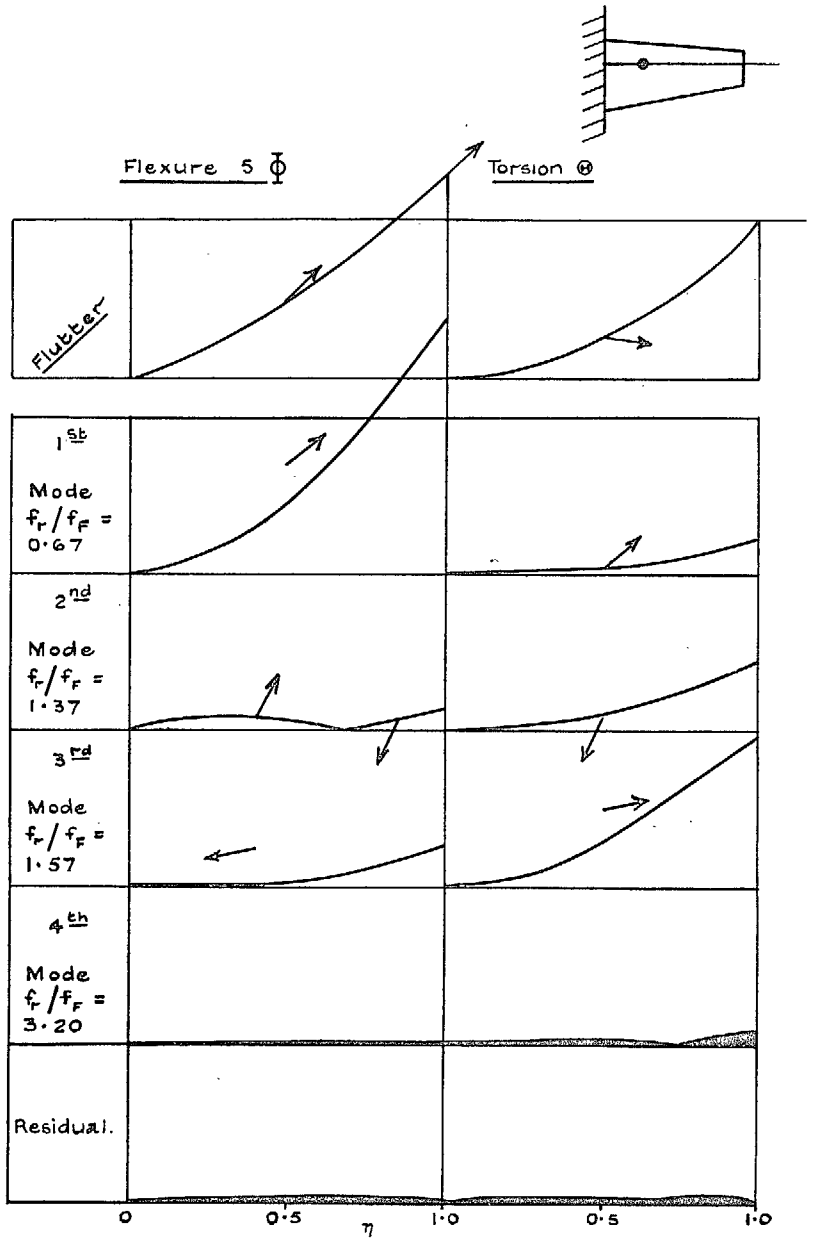

FIG. 15. Flutter mode resolved into normal mode components. Mass added internally (condition I_1).

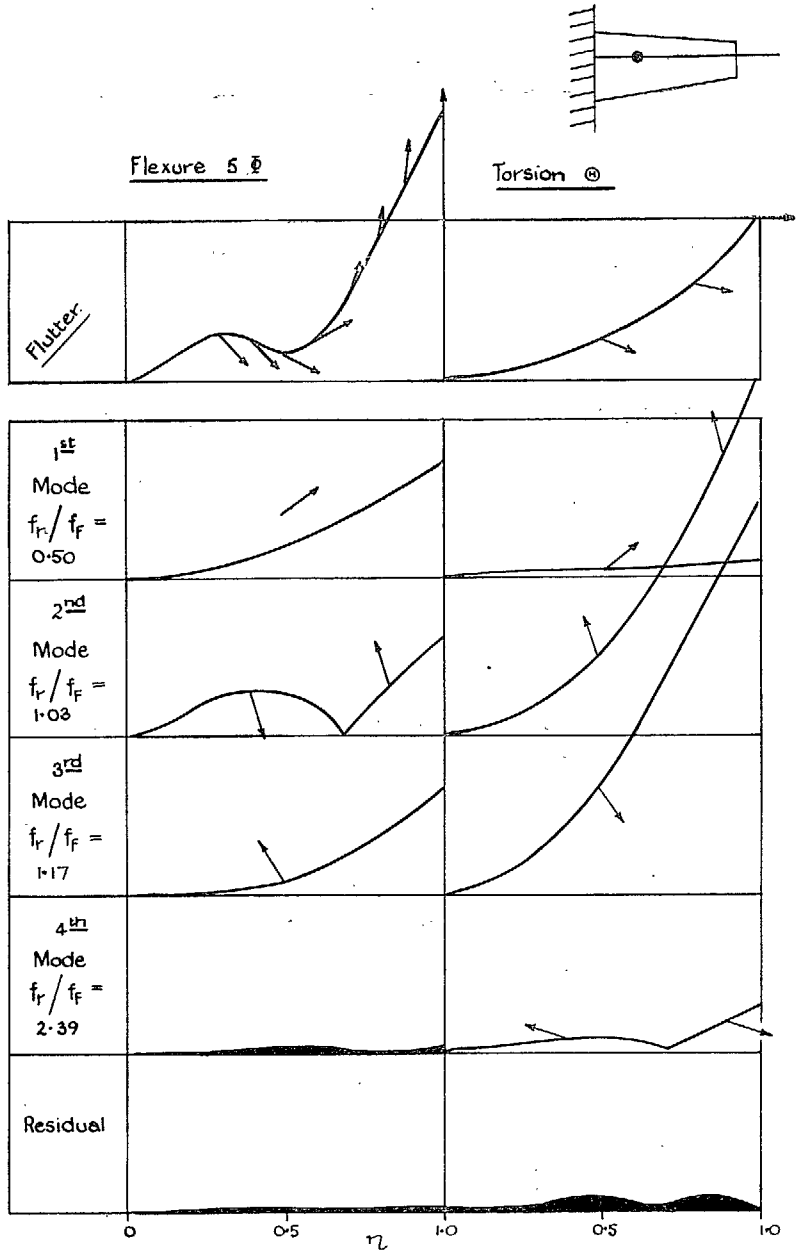

FIG. 16. Flutter mode resolved into normal mode components. Mass added internally (condition I_2).

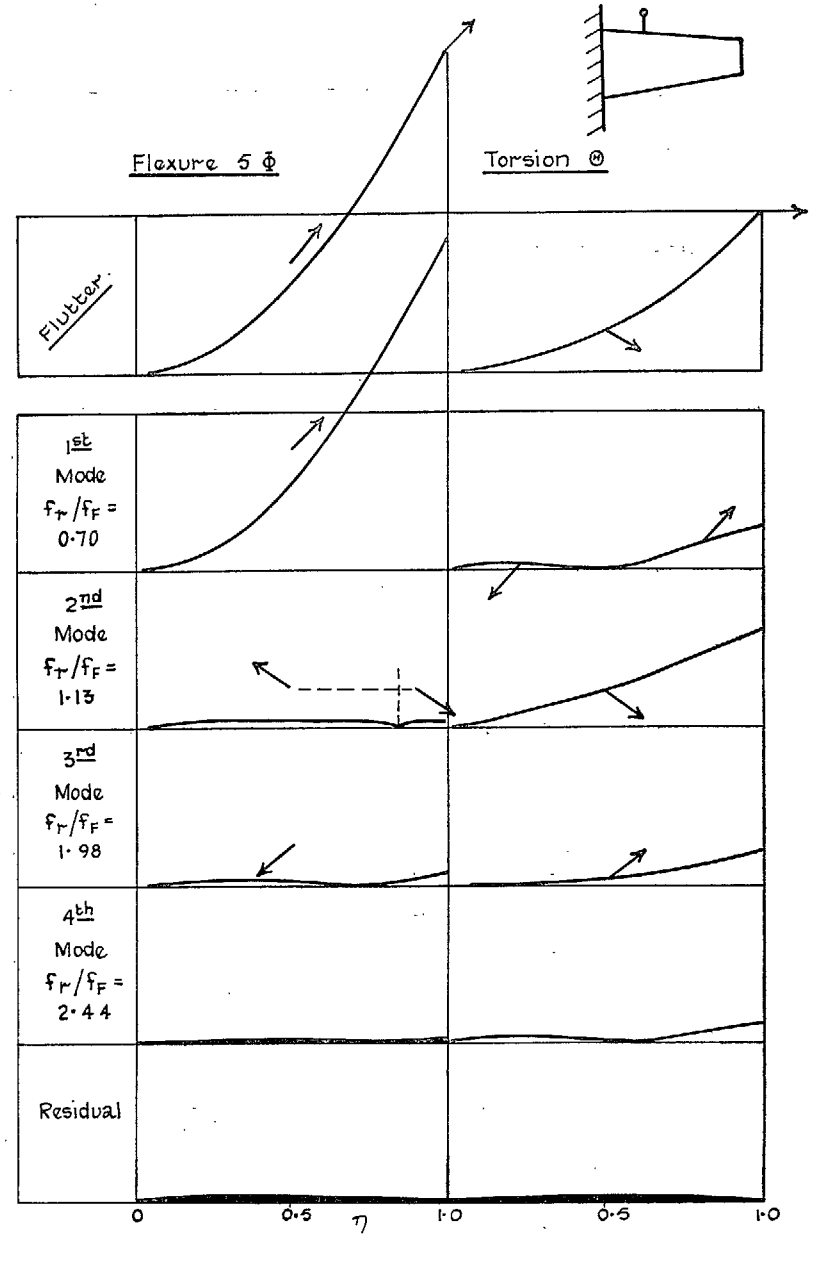

FIG. 17. Flutter mode resolved into normal mode components. Mass added externally (condition E_1).

J4316 18/9296 K9 5/55 D&Co. 34/263

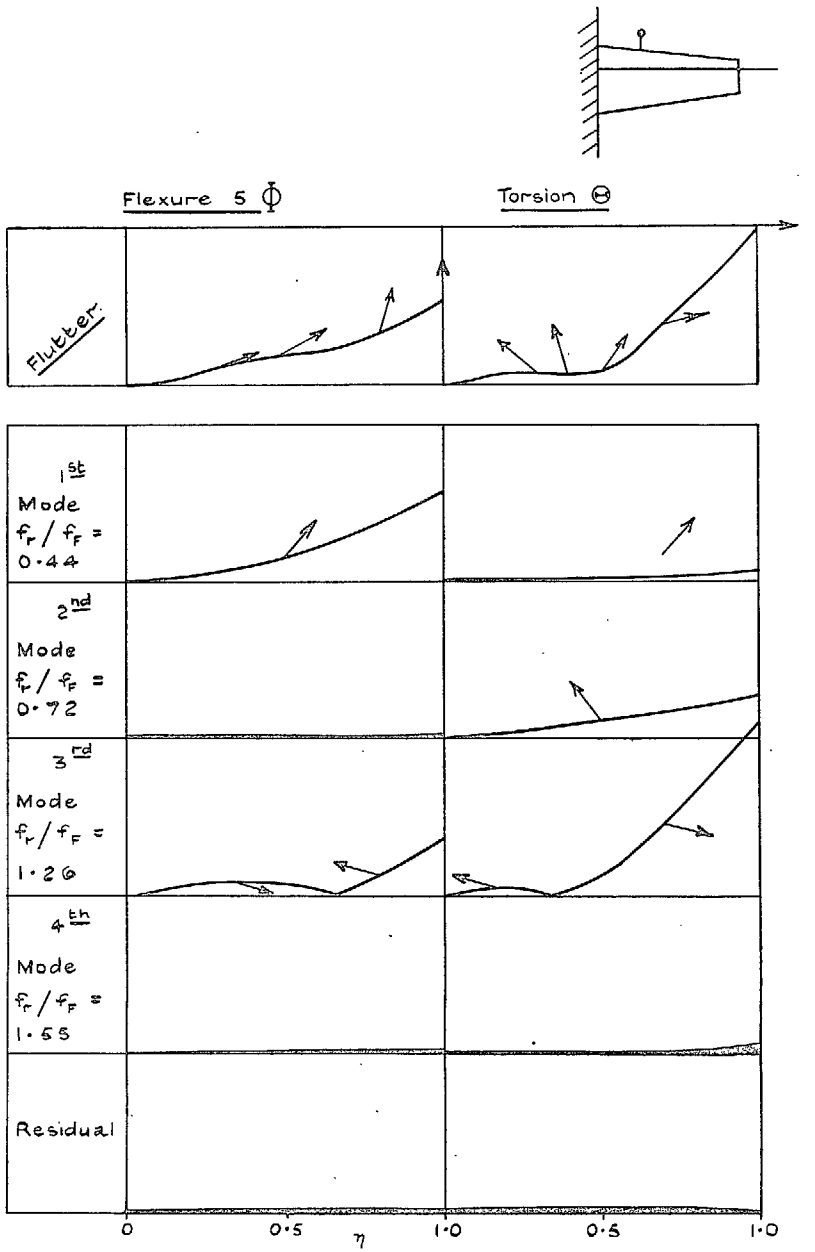

FIG. 18. Flutter mode resolved into normal mode components. Mass added externally (condition E_2).

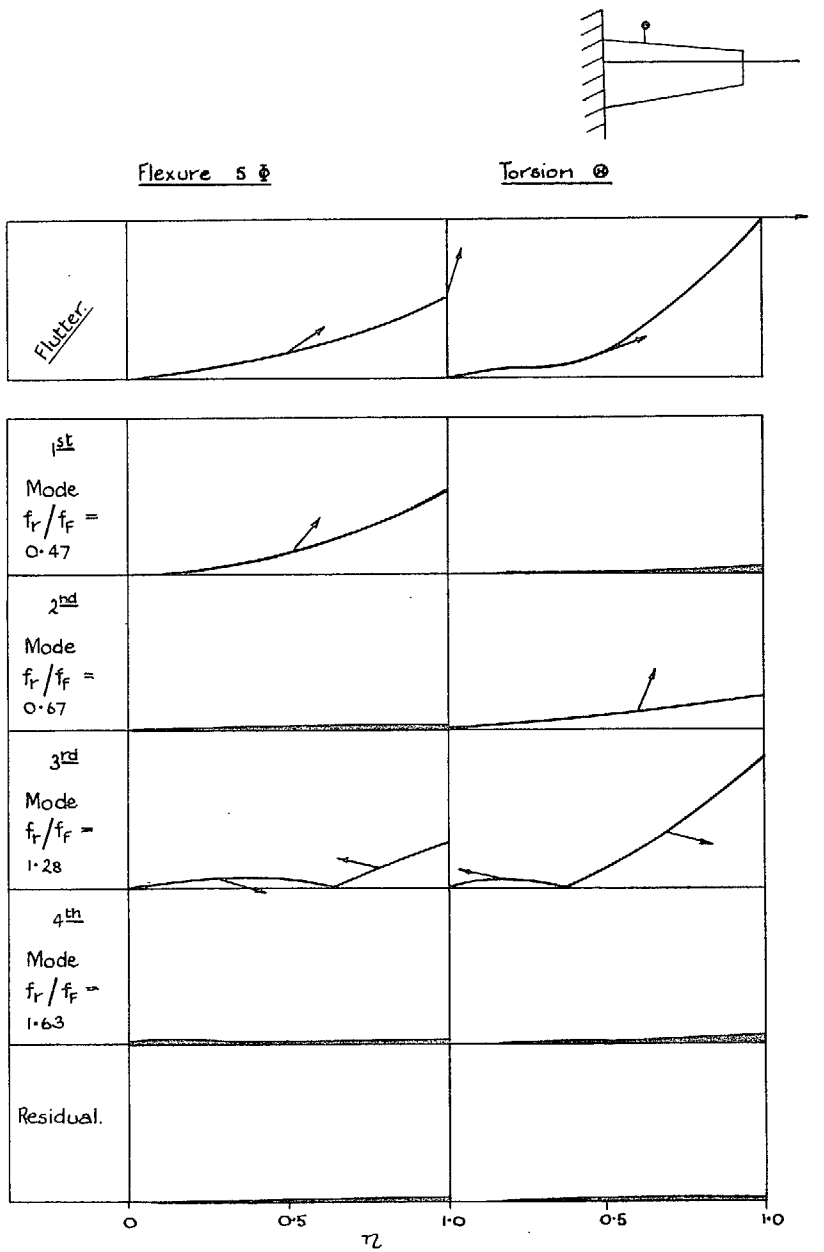

FIG. 19. Flutter mode resolved into normal mode components. Mass added externally (condition E_3).

PRINTED IN GREAT BRITAIN

Publications of the Aeronautical Research Council

ANNUAL TECHNICAL REPORTS OF THE AERONAUTICAL RESEARCH COUNCIL (BOUND VOLUMES)

1936 Vol. I. Aerodynamics General, Performance, Airscrews, Flutter and Spinning. 40*s*. (41*s*. 1*d*).

Vol. II. Stability and Control, Structures, Seaplanes, Engines, etc. 50*s*. (51*s*. 1*d*.)

1937 Vol. I. Aerodynamics General, Performance, Airscrews, Flutter and Spinning. 40*s*. (41*s*. 1*d*.)

Vol. II. Stability and Control, Structures, Seaplanes, Engines, etc. 60*s*. (61*s*. 1*d*.)

1938 Vol. I. Aerodynamics General, Performance, Airscrews. 50*s*. (51*s*. 1*d*.)

Vol. II. Stability and Control, Flutter, Structures, Seaplanes, Wind Tunnels, Materials. 30*s*. (31*s*. 1*d*.)

1939 Vol. I. Aerodynamics General, Performance, Airscrews, Engines. 50*s*. (51*s*. 1*d*.)

Vol. II. Stability and Control, Flutter and Vibration, Instruments, Structures, Seaplanes, etc. 63*s*. (64*s*. 2*d*.)

1940 Aero and Hydrodynamics, Aerofoils, Airscrews, Engines, Flutter, Icing, Stability and Control, Structures, and a miscellaneous section. 50*s*. (51*s*. 1*d*.)

1941 Aero and Hydrodynamics, Aerofoils, Airscrews, Engines, Flutter, Stability and Control, Structures. 63*s*. (64*s*. 2*d*.)

1942 Vol. I. Aero and Hydrodynamics, Aerofoils, Airscrews, Engines. 75*s*. (76*s*. 3*d*.)

Vol. II. Noise, Parachutes, Stability and Control, Structures, Vibration, Wind Tunnels. 47*s*. 6*d*. (48*s*. 7*d*.)

1943 Vol. I. Aerodynamics, Aerofoils, Airscrews, 80*s*. (81*s*. 4*d*.)

Vol. II. Engines, Flutter, Materials, Parachutes, Performance, Stability and Control, Structures. 90*s*. (91*s*. 6*d*.)

1944 Vol. I. Aero and Hydrodynamics, Aerofoils, Aircraft, Airscrews, Controls. 84*s*. (85*s*. 8*d*.)

Vol. II. Flutter and Vibration, Materials, Miscellaneous, Navigation, Parachutes, Performance, Plates, and Panels, Stability, Structures, Test Equipment, Wind Tunnels. 84*s*. (85*s*. 8*d*.)

ANNUAL REPORTS OF THE AERONAUTICAL RESEARCH COUNCIL—

1933–34	1*s*. 6*d*. (1*s*. 8*d*.)	1937	2*s*. (2*s*. 2*d*.)
1934–35	1*s*. 6*d*. (1*s*. 8*d*.)	1938	1*s*. 6*d*. (1*s*. 8*d*.)
April 1, 1935 to Dec. 31, 1936.	4*s*. (4*s*. 4*d*.)	1939–48	3*s*. (3*s*. 2*d*.)

INDEX TO ALL REPORTS AND MEMORANDA PUBLISHED IN THE ANNUAL TECHNICAL REPORTS, AND SEPARATELY—

April, 1950 – – – – R. & M. No. 2600. 2*s*. 6*d*. (2*s*. 7½*d*.)

AUTHOR INDEX TO ALL REPORTS AND MEMORANDA OF THE AERONAUTICAL RESEARCH COUNCIL—

1909–1949 – – – – – R. & M. No. 2570. 15*s*. (15*s*. 3*d*.)

INDEXES TO THE TECHNICAL REPORTS OF THE AERONAUTICAL RESEARCH COUNCIL—

December 1, 1936 — June 30, 1939.	R. & M. No. 1850.	1*s*. 3*d*. (1*s*. 4½*d*.)
July 1, 1939 — June 30, 1945.	R. & M. No. 1950.	1*s*. (1*s*. 1½*d*.)
July 1, 1945 — June 30, 1946.	R. & M. No. 2050.	1*s*. (1*s*. 1½*d*.)
July 1, 1946 — December 31, 1946.	R. & M. No. 2150.	1*s*. 3*d*. (1*s*. 4½*d*.)
January 1, 1947 — June 30, 1947.	R. & M. No. 2250.	1*s*. 3*d*. (1*s*. 4½*d*.)
July, 1951 – – – –	R. & M. No. 2350.	1*s*. 9*d*. (1*s*. 10½*d*.)

Prices in brackets include postage.

Obtainable from

HER MAJESTY'S STATIONERY OFFICE

York House, Kingsway, London W.C.2 ; 423 Oxford Street, London W.1 (Post Orders : P.O. Box No. 569, London S.E.1) ; 13A Castle Street, Edinburgh 2 ; 39 King Street, Manchester 2 ; 2 Edmund Street, Birmingham 3 ; 109 St. Mary Street, Cardiff ; Tower Lane, Bristol 1 ; 80 Chichester Street, Belfast OR THROUGH ANY BOOKSELLER

S.O. Code No. 23-2866